UNCLASSIFIED

AD NUMBER
AD378127
CLASSIFICATION CHANGES
TO: unclassified
FROM: confidential
LIMITATION CHANGES
TO: Approved for public release, distribution unlimited
FROM: Distribution authorized to U.S. Gov't. agencies and their contractors; Administrative/Operational Use; Nov 1966. Other requests shall be referred to Naval Research Laboratory, Washington, DC 20375.
AUTHORITY
31 Dec 1969, GDS, DoD 5200.1-R; NRL ltr, 22 Jan 2004

THIS PAGE IS UNCLASSIFIED

GENERAL DECLASSIFICATION SCHEDULE

IN ACCORDANCE WITH
DOD 5200.1-R & EXECUTIVE ORDER 11652

THIS DOCUMENT IS:

CLASSIFIED BY _____

Subject to General Declassification Schedule of Executive Order 11652-Automatically Downgraded at 2 Years Intervals- DECLASSIFIED ON DECEMBER 31, 1969

BY

Defense Documentation Center
Defense Supply Agency
Cameron Station
Alexandria, Virginia 22314

DISCLAIMER NOTICE

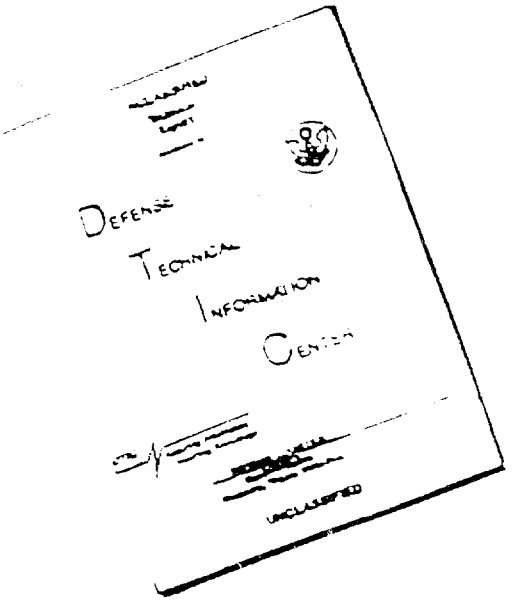

THIS DOCUMENT IS BEST QUALITY AVAILABLE. THE COPY FURNISHED TO DTIC CONTAINED A SIGNIFICANT NUMBER OF PAGES WHICH DO NOT REPRODUCE LEGIBLY.

SECURITY MARKING

The classified or limited status of this report applies to each page, unless otherwise marked.
Separate page printouts MUST be marked accordingly.

THIS DOCUMENT CONTAINS INFORMATION AFFECTING THE NATIONAL DEFENSE OF THE UNITED STATES WITHIN THE MEANING OF THE ESPIONAGE LAWS, TITLE 18, U.S.C., SECTIONS 793 AND 794. THE TRANSMISSION OR THE REVELATION OF ITS CONTENTS IN ANY MANNER TO AN UNAUTHORIZED PERSON IS PROHIBITED BY LAW.

NOTICE: When government or other drawings, specifications or other data are used for any purpose other than in connection with a definitely related government procurement operation, the U. S. Government thereby incurs no responsibility, nor any obligation whatsoever; and the fact that the Government may have formulated, furnished, or in any way supplied the said drawings, specifications, or other data is not to be regarded by implication or otherwise as in any manner licensing the holder or any other person or corporation, or conveying any rights or permission to manufacture, use or sell any patented invention that may in any way be related thereto.

CONFIDENTIAL

NRL Memorandum Report 1730

Power Limitations and Fidelity of Acoustic Sources

[Unclassified Title]

R. H. Ferris and F. L. Hunsicker

Propagation Branch
Sound Division

November 1966

NAVAL RESEARCH LABORATORY
Washington, D.C.

CONFIDENTIAL

Downgraded at 3 year intervals.
Declassified after 12 years.

SECURITY

This document contains information affecting the national defense of the United States within the meaning of the Espionage Laws, Title 18, U.S.C., Sections 793 and 794. The transmission or revelation of its contents in any manner to an unauthorized person is prohibited by law.

CONTENTS

Abstract ii
Problem Status ii
Authorization ii

INTRODUCTION 1

EFFECT OF ACOUSTIC LOADING ON POWER LIMITATION 2

General 2
Analog Technique 3
Results of Measurements on the ARTEMIS Source 7

PHASE AND AMPLITUDE DISTORTION 11

General 11
Sine-wave Measurements of the Transfer Function for the ARTEMIS Source 13
Measurement of the Transfer Function Using Pseudorandom-Sequence Signals 15
Cross-Correlation Function Measurements 24

SUMMARY 26

ABSTRACT
(Unclassified)

The generation of a high-intensity acoustic field which is a faithful replica, or at least a known function, of the input signal is a prime requirement in modern active sonar systems. Most sonar signals in use are modulated sine waves. Therefore, transducers must be capable of efficiently transforming this type of signal. It is evident that design criteria and test procedures based on steady-state sine-wave signals are not adequate. The potential gain in sonar performance to be realized by maximizing signal power without distortion merits increased effort addressed to this problem.

This report is intended to point out some of the problems associated with the generation of maximum-energy acoustic fields by large multielement sources and to suggest techniques of analysis and testing. The use of electrical analog analysis of power-limiting factors in transducer elements appears to be an attractive method if a means can be developed for estimating the range of acoustic-loading values experienced by elements in an active array.

A description of calibration procedures used and results obtained in tests of the ARTEMIS acoustic source are presented to serve as an example of proposed test methods.

PROBLEM STATUS

This is an interim report on one phase of this project. Work is continuing.

AUTHORIZATION

NRL Problem 55S01-23
Projects RF 101-03-44-4066
and SF 101-03-16-11223

INTRODUCTION

Most acoustic generators of practical interest in sonar employ modulated sine-wave signals to convey information. The simplest form of modulation is widely used in echo ranging and consists of a sinusoidal signal which is gated on periodically to produce pulses of energy having typical time durations corresponding to a large number of cycles of the modulated wave. The probability of detecting a signal in the background noise increases with increased signal energy. Signal energy can be increased by increasing signal power or duration, or both. When a target echo contains sufficient doppler shift to permit discrimination between signal and reverberation, the simple gated sine-wave signal is well suited for detection. Increasing pulse duration and power enhances performance. Accurate location of the target in range, however, sets a limit on the pulse duration depending on the resolution requirements. Beyond that point, signal energy can be increased only by increasing power or by increased focusing of the energy in the direction of the target. The use of nonperiodic signals, together with coherent processing, eliminates the dependence of bandwidth on pulse length and therefore permits the use of long-duration signals with acceptable range resolution. Such signals are also effective against low doppler targets. Signal energy cannot be indefinitely increased by increasing signal duration due to the temporal-stability limitation of the propagation path. Therefore, with either gated sine-wave or the nonperiodic signals, it is desirable to maximize signal power. In systems employing coherent processing, this must be accomplished with a minimum of phase and amplitude distortion over the frequency band containing the signal.

As the power input to a transducer is increased, all factors in the transducer element, such as potentials, currents, temperatures, pressures, and mechanical stress, approach their limiting values, which, if exceeded, will either cause failure of the element or cause it to operate in an unacceptably nonlinear fashion. That factor which first reaches its limit defines the maximum allowable power input to the transducer. If operating conditions, such as acoustic loading, ambient pressure or temperature, or type of signal used, are changed, there may be a change in the power-limiting factor. All the power-limiting factors, with the exception of certain thermal conditions, are sensitive to peak rather than average values. In general, the transient response of a single element or an element operating in an array of elements is such that it is difficult to determine the peak values of power-limiting factors analytically and, in most cases, it is equally difficult to measure them experimentally. In practice, the failure of an element is frequently the first

indication that a limiting value has been reached. Information obtained in this manner, however, is not necessarily valid if operating conditions have changed. On the other hand, if transducer elements are not operated at power levels close to their limit, system performance is degraded by the use of less-than-maximum available signal power. Clearly, a need exists for

1. Increasing knowledge of the causes of power limitations in acoustic sources,

2. Developing nondestructive techniques of determining power limitations in existing transducers,

3. Establishing design criteria for optimizing power capability of sources to be used with particular signal types, and

4. Specifying techniques for testing sources for phase and amplitude distortion.

This report is intended to call attention to the importance of these four areas to optimized sonar performance and to report on limited investigations which lead to conclusions and recommendations on certain aspects of the problem and to point out examples of problem areas in other facets.

EFFECT OF ACOUSTIC LOADING ON POWER LIMITATION

General

An acoustic projector having dimensions which are appreciable compared to the sound wavelength in water cannot, in general, experience a uniform acoustic load over its radiating surface due to acoustic interactions. Since all large projectors are composed of a large number of individual transducer elements, there is a variation in loading from element to element. In the steady-state condition, the loading pattern is fixed and can be calculated,[1] although it might be necessary to make various simplifying assumptions in order to restrict the complexity of the calculation to a form compatible with available computers. Figure 1[2] illustrates the steady-state loading pattern calculated for one quadrant of a 2-1/2λ by 4λ rectangular plane array in which the simplifying condition of a uniform velocity

---

1. R. V. Baier, "Theoretical Interaction Computations for Transducer Arrays, Including the Effects of Several Different Types of Electrical Terminal Connections", NRL Conf Report 6314, Oct 1965
2. R. H. Ferris, R. V. Baier, "Acoustic Interaction in Multielement Sonar Arrays", Proceedings of the Seventh Navy Science Symposium, ONR-16, vol. 2, May 1963 (Conf)

over the face of the array was assumed. It can be seen that very small elements in such an array would experience wide variations in loading, depending on their position in the array. Larger elements would tend to average the loading on their individual radiating faces and thus would be subjected to a lesser variation. It is possible, however, that the larger elements could be adversely affected by unsymmetric loading. In contrast to the steady-state problem, a complete analytical solution for the conditions encountered with modulated signals is, in the present state of the art, unthinkable. Fortunately, a complete solution is not required in order to determine the power-limiting effects of the loading variations. It is sufficient to know the range of possible complex loadings. When the behavior of an element is examined over this range, the worst case can be assumed to be the limiting condition, since the allowable power input to the array is limited by the worst-case element. Although a technique of estimating the range of loading encountered with modulated signals is not in hand, it appears to be a more tractable problem than a complete analytical solution.

A possible approach to investigating the effects of loading on power-handling capability is to instrument a sample of elements to record the instantaneous response of each of the factors which might limit power while the full array is being driven with the particular modulated signals to be used in the system of which the projector is a part. This approach has some obvious disadvantages in that the required instrumentation would generally require a major modification of the elements and tests must be made on the completed source. A second approach would be to instrument a single element on which the dynamic load can be varied over the required range by some technique such as the standing-wave tube or dynamically driven load elements. A third approach which is applicable to some transducers involves the use of an electrical analog circuit. If such a circuit can be constructed to accurately represent an element, measurement of the power-limiting factors is greatly simplified and loading is completely and readily controllable. An example of this technique will now be shown.

Analog Technique

Figure 2 illustrates the basic configuration of an illustrative ceramic element. It consists of a piezoelectric ceramic stack having a reaction mass bonded to one end and a radiating mass bonded to the other end. A third mass, the watertight housing, is joined to the radiating mass with a pressure-release gasket. The ceramic

stack acts as a spring between the reacting and radiating masses, and the pressure-release gasket acts as a spring between the radiating mass and the housing. Figure 3 illustrates the equivalent circuit of this element being driven from an amplifier having an internal impedance R. The analog circuit was assembled and measurements made of various possible power-limiting factors. In this circuit the analog voltage is equivalent to force and current to velocity. To exemplify the analysis technique, several possible power-limiting factors were selected and their amplitudes recorded as the analog circuit was driven by continuous-wave and modulated waveforms. The specific factors selected were

1. The mechanical stress in the ceramic, given by

$$\sigma_c = \frac{\beta}{A_c} V_{c_1},$$

where

V_{c_1} is the voltage across capacitor c_1,

A_c is the area of the ceramic material, and

β is the electromechanical turns ratio.

2. The mechanical stress in the pressure-release material between the radiating and housing masses, given by

$$\rho_b = \frac{\beta}{A_b} V_{c_3},$$

where

V_{c_3} is the voltage across capacitor c_3,

A_b is the area of the pressure-release material, and

β is the electromechanical turns ratio.

3. The potential gradient in the ceramic, given by

$$E_g = \frac{V_{c_o}}{d} ,$$

where

V_{c_o} is the voltage across capacitor c_o, and

d is the thickness of one ceramic disk.

For illustrative purposes, maximum allowable values for each of these three factors were arbitrarily selected and corresponding peak values of electrical potentials across the appropriate components in the analog circuit were computed from the given equations. Each of the three potentials was held constant in turn at the computed values as the circuit was driven by steady-state continuous-wave signals which were stepped in frequency across the operating band. During this procedure the voltage input was recorded. The assumed limiting values were 125-pounds-per-square-inch stress in the ceramic, 25-pounds-per-square-inch stress in the pressure-release material, and a maximum potential E across the ceramic stack of 1000 volts.

This process was repeated for various equivalent values of acoustic load, as given in Table 1.

TABLE 1

Real Part/ρcA	Reactive Part/ρcA
0.0	-0.5
0.0	0.0
0.0	+0.5
0.1	-0.5
0.1	0.0
0.1	+0.5
0.5	-0.5
0.5	0.0
0.5	+0.5
1.0	-0.5
1.0	0.0
1.0	+0.5

A positive reactive load represents mass loading and a negative sign represents stiffness loading.

The results are plotted in Fig. 4, where voltage input is plotted as a function of frequency. These curves illustrate the maximum allowable steady-state input voltage as determined by the worst-case loading condition of the three factors investigated. The curves in Fig. 4 represent the power limitation imposed by the factors' stress in the ceramic, stress in the band, and potential gradient in the ceramic. Although the power output of an element depends upon the acoustic load seen by that particular element as well as the driving voltage, the total power output of an array of parallel-connected elements having a fixed loading distribution is limited by the maximum allowable voltage drive to the worst-case element. It can be observed that, for the assumed limiting values of the three factors, the power output is not always limited by the same factor. If, as in this example, it was determined that the steady-state loading at various points in an array of these elements varied over the limits of 0.0 to 1.0 for the real part and -0.5 to 0.5 for the reactive part, the power input would be limited by potential gradient between 4.0 and 4.43 kilohertz, by stress in the ceramic between 4.43 and 4.72 kilohertz, and by stress in the pressure release for higher frequencies.

A comparable analysis for modulated waveforms is complicated by the fact that with modulated signals the interaction field seen by an element is nonperiodic. A possible approach is to estimate the range over which the load can vary both in time and position and provide a dynamic load for the analog circuit which varies in a random fashion within the limits of this range. The modulated signal input to the analog circuit could then be increased in value until the peak value of the factor being investigated reached its limiting value at least once. It is possible that the value of the maximum allowable input voltage obtained in this statistical manner would be somewhat lower than that required in a real array. On the other hand, an approximate analysis can be made utilizing a selection of fixed loads, as was done in the steady-state case. The approximation could be expected to degrade as the signal bandwidth is increased. The method employing dynamically varying loads has not been investigated experimentally. However, measurements of maximum input voltage were obtained for modulated signals employing a selection of fixed loads to compare with the steady-state measurements performed with the analog circuit shown in Fig. 3. Pulsed continuous-wave and phase-reversal modulated pseudorandom sequences in which the modulation code was generated by a linear shift register were used. Ceramic strain was assumed to be the limiting factor.

The input level was increased until the peak value of the ceramic strain reached the limiting value, at which time the root-mean-square voltage input was recorded. The results are listed in Table 2. The carrier frequency in each case was five kilohertz. The first column lists the type of modulation used, the second column the resistive acoustic load, and the third column the reduction in allowable input voltage when compared with continuous-wave operation under the same conditions.

TABLE 2

Type of Modulation	Acoustic Load	Reduction in Allowable Input Level Ref. to Steady State
Pulsed continuous wave	1.0 pcA	3.0 db
Pulsed continuous wave	0.1 pcA	5.0 db
Phase-modulated PRS	1.0 pcA	6.0 db
Phase-modulated PRS	0.1 pcA	11.8 db

Results of Measurements on the ARTEMIS Source

During initial tests[3] of the partially completed ARTEMIS acoustic source in May 1961, more than 40 percent of the transducer elements failed when the array was driven at a power level below the design value. At the time of this test, only one-tenth of the elements had been installed, resulting in an array approximately one wavelength square. In the investigation of the cause of the element failures, accelerometers were employed to obtain information on the displacement amplitudes of the radiating faces of the individual elements. A large variation in displacement amplitudes was observed with many of the elements having displacements far in excess of predicted values based on radiated power of the array. The ARTEMIS elements are of the variable-reluctance type having two masses and connecting springs. The element radiating face is a square plane with the length of the sides approximately 1/12 wavelength in water. Examination of the damaged elements revealed that the transducer springs had broken due to excessive deflection. Computer analysis, which was performed at a later date, disclosed that, with elements of this small size, a large variation in acoustic loading among the elements

3. A. T. McClinton, R. H. Ferris, W. A. Herrington; "Project ARTEMIS High Power Acoustic Source, Interim Report on Acoustic Performance"; NRL Memorandum Report 1205, Aug 1961 (Conf)

could be expected due to acoustic interactions. The deleterious effect of interactions[4] was heightened by the electrical connection of elements in which the elements were divided into groups of six with a series connection of elements within each group and a parallel connection of groups. Since the input impedance of an element increases when the element becomes unloaded, the series connection resulted in increased power being applied to unloaded elements in a group, thus further increasing their deflections. A subsequent modification[5] placed all elements in a parallel connection, and this greatly improved the velocity distribution but not to the extent where full design power could be applied to the array. A computer analysis indicated that the real part of the radiation loading in a one-wavelength-square, parallel-connected array would vary in the range from -0.1 to +0.9 ρcA. The computation was performed also for the full-scale 2-1/2λ-by-4λ array. However, in this case, the computer and computation techniques utilized necessitated assuming an equal velocity for all elements. The latter computation resulted in a range of values for the real part of the radiation loading of 0.2 to 1.01 ρcA. All computations were based on steady-state sinusoidal drive.

It was evident from the observed failures that the critical factor which imposed a limitation on operating power level was the transducer-element springs. No information was available as to the actual deflections experienced by the springs under various loading conditions and types of input signals other than that the permissible deflections were being exceeded at an unpredicted low level of drive as evidenced by the failures. A program was then initiated to investigate the actual spring deflections by modifying a group of elements by the installation of accelerometers on the two-element masses in appropriate positions, such that the spring deflections could be computed from the observed relative motion of the masses. Installation of the accelerometers required disassembly and reassembly of the elements, since the springs and the reaction mass are completely enclosed within the radiating mass, which serves as an outer housing. Tests[4] were made of the completed ARTEMIS source in which these specially instrumented elements were inserted sequentially in approximately 150 locations scattered over the extent of the array. Steady-state measurements were performed at small increments of frequency in the range from 350 to 500 hertz. The operating band for the ARTEMIS source is 350 to 450 hertz. The mean and maximum observed spring deflections are plotted in Fig. 5. It can be seen that the ratio of the maximum to the mean is particularly high at the upper end of the frequency band and at frequencies in the neighborhood of 400 hertz.

---

4. R. H. Ferris; "Project ARTEMIS High Power Acoustic Source, Fourth Interim Report on Acoustic Performance", NRL Memorandum Report 1400, Mar 1963 (Conf)
5. R. H. Ferris; "Test of Project ARTEMIS Acoustic Source", NRL Memorandum Report 1648, Sep 1965 (Conf)

The ratio at 450 hertz is approximately 2-1/2 to 1, which results in a reduction in allowable input power of about eight decibels relative to the power which would be acceptable if all spring deflections were uniform and equal to the mean. Other studies have shown that the deflection variation is principally due to the nonuniform loading, although a rotary motion[5] of the inner mass accounts for some of the spread. The rotary motion is particularly pronounced at frequencies in the neighborhood of 400 hertz.

The maximum permissible spring deflection is approximately 0.010 inch peak to peak. At higher deflections they are subject to fatigue failures. Applying the spring deflection limitation to the data of Fig. 5, the data of Fig. 6 were derived. This figure illustrates, as a function of frequency, the relative permissible voltage input to the amplifiers. Absolute values of voltage input are not given, since the preamplifier gain can be varied over wide limits. Finally, the maximum safe source level can be computed for steady-state operation by combining acoustic calibration data with the spring deflection data. This information is plotted in Fig. 7. A similar plot can be made for the maximum permissible power input to the transducer. The power input data have been supplied to the users of the source as a guide to prevent damage to the elements. A suitable safety factor has been included to account for error due to the size of the statistical sample from which these data were derived and to allow for overshoots, which it will be shown can occur when the signal is gated on or off.

The analog technique of analysis described in an earlier section also was applied to the ARTEMIS source element. The equivalent analog circuit shown in Fig. 8 was constructed and tested in the laboratory under steady-state conditions. The range of values for acoustic loading was estimated to be from 0 to 1.0 pcA for the real part and from -0.3 to +0.3 pcA for the reactive part. The simulated load on the analog circuit was ranged over these values as the frequency was stepped over the operating band. The input voltage was maintained at values which produced a constant simulated spring deflection of 7.07 mils peak to peak, This value of spring deflection results from applying a three-decibel safety factor to the limiting value of ten mils. The value of the input voltage required to maintain the constant spring deflection was recorded. At each frequency, the minimum value of input voltage, depending on load, was selected and input powers to the array calculated corresponding to the selected element voltages. This power represents the predicted

---

5. "See footnote 5 on p. 8."

maximum allowable input power to the array. The results are plotted in Fig. 9, along with the curve of maximum allowable input power determined from experimental measurements with specially instrumented elements in the field. The third curve illustrates the predicted maximum allowable input power for the condition of uniform loading having a value of unity ρcA with no reactive loading. The dip in the experimental curve at 400 cycles per second results from the excitation of a rotary mode of vibration in the element. This exemplifies a shortcoming in the analog circuit analysis in that the equivalent circuit did not include this degree of freedom. The two curves are in reasonable agreement otherwise when it is considered that they are both subject to inherent errors. The principal uncertainty in the experimental curve results from the small size of the statistical sample of elements; i.e., approximately ten percent of the elements were instrumented. On the other hand, the analog data suffer from the lack of certainty concerning the range and combination of real and imaginary components of acoustic loading values and the approximation of the equivalent circuit to the actual element. For the analog technique to have real value in predicting available power levels, a method must be developed for accurately estimating the limiting bounds of acoustic loading.

The maximum allowable input power to the ARTEMIS source as defined in Fig. 9 refers to steady-state sinusoidal drive. This type of operation has no practical interest in sonar, nor can it be assumed that the same power limitations apply to modulated signals. The spring deflections of 20 elements of the ARTEMIS source array were monitored while the array was driven with a shift-register-generated pseudorandom sequence. It was observed that occasional large peak spring deflections occurred in each element. Measurement of these peak values disclosed that the maximum safe input power for this type of signal was less than the maximum allowable steady-state input with a sinusoidal signal. The pseudorandom signal (i.e., PRS) employed was of the phase-reversal modulated type which has a peak-to-rms ratio only slightly greater than a sine wave. The maximum allowable PRS powers, as determined from experimental measurements on the array and from the analog circuit tests with the assumed loading are plotted as points in Fig. 9. It can be seen that the two methods agree within one decibel. This is surprisingly good agreement, considering that only fixed loads, whose range of values was derived from steady-state computations, were used. Further studies concerning the nature of transient loading effects are needed before conclusions can be drawn regarding the adequacy of this technique.

PHASE AND AMPLITUDE DISTORTION

General

The effectiveness of coherent processing techniques depends upon having complete knowledge of the transmitted signal. In addition to the normal calibration procedures, the complex transfer function should be measured for any acoustic source which is to be used in a coherent system. The measurements should be made on the entire source system, including filters, preamplifier, power amplifier, load-matching components, and transducer. Ideally, the entire system should be tested together under operating conditions. By repeating the measurements at several power levels from less than one percent of full power to full power, the linearity can be determined. If the system is linear, sine-wave measurements at small increments of frequency throughout the operating band will suffice to define the system characteristics for all signal types. On the other hand, if significant non-linearity is observed, the transfer function must be obtained by spectral analysis with the types of signals of intended use.

The measurement of source transfer function requires that a monitoring hydrophone be held in a fixed position relative to the acoustic source and the position be accurately known. At high frequencies, the required degree of stability is difficult to achieve. For example, a system operating at a frequency of five kilohertz would require that the hydrophone maintain its position constant relative to the source to within one-sixth of an inch in range in order to maintain a phase stability of five degrees. The hydrophone distance from the source must be sufficient to obtain an approximation of far-field characteristics to the desired degree of accuracy.

The transfer function of the ARTEMIS acoustic source was measured at sea during November 1965. During these tests the source ship, the USNS MISSION CAPISTRANO (T-AG 162), was lying to in the sheltered waters of Northwest Providence Channel with the transducer array submerged to a depth of 600 feet. Three hydrophones were mounted on a spar which was affixed to the end of a 190-foot boom. The boom was pivoted at the base of the transducer array in such a manner that the hydrophones could be held rigidly in front of the array in several fixed positions in a vertical plane through the acoustic axis. Since the highest frequency of interest was 500 hertz, it was necessary to hold a positional stability to within approximately two inches in order to maintain a phase stability of five degrees. Although the

stiffness of the boom was not sufficient to guaranty this degree of stability in an environment of fluctuating currents, steady-state measurements revealed no measurable phase fluctuations which could be attributed to hydrophone motion. However, attempts to repeat measurements after the boom had been moved resulted in phase differences as great as 12 degrees, part of which might be attributable to deviation in hydrophone position, with the remainder probably due to temperature variations. The resolution of the phase-measuring instrumentation was one degree. The range from the center of the array to the hydrophones varied from 189 to 200 feet, depending on the boom angle. These ranges provide a good approximation to far-field conditions for the magnitude of the acoustic field in the major lobe. Figure 10 illustrates the computed 400-hertz directivity patterns in a vertical plane perpendicular to the plane of the array for a uniformly vibrating plane rectangular piston 30 feet wide by 50 feet high, corresponding to the dimensions of the ARTEMIS source. The solid lines represent the computed far-field amplitude and phase patterns, whereas the dashed lines depict the computed near-field patterns. The far-field values were computed for a constant range and referenced to zero decibels in magnitude and zero degrees in phase on the acoustic axis. The near-field data were computed at ranges from the center of the array corresponding to the actual hydrophone ranges and then referenced to the same range as the far-field patterns in order to provide a direct comparison between the values which would be obtained from an ideal transducer at the ranges employed and in the far field. It can be seen that the hydrophone ranges are sufficient to approximate the far-field intensity to within 0.5 decibel for angles less than ten degrees with respect to the acoustic axis. However, the limited range does distort the nulls considerably. The computed near-field phase pattern differs from the far-field pattern by approximately 20 degrees in that portion of the major lobe located between the half power points. This phase lag results from the increased range between element and hydrophone with increased distance of the element from the center of the array. As the hydrophone is moved away from the acoustic axis, those elements having decreasing phase lag due to decreasing range contribute an increasing share of the intensity and, thus, the near-field phase exhibits a decreasing lag relative to the far-field phase. In Fig. 11, the difference between the computed near-field phase, at hydrophone distance on the acoustic axis, and the equivalent far-field phase is plotted as a function of frequency for on axis and six degrees below axis, as shown by the solid lines. The dotted lines, which represent linear phase shifts, are plotted for comparative purposes. It can be seen that the phase error caused by the finite hydrophone range is very nearly a linear

function of frequency, representing a time or range shift, and therefore does not distort the form of the transfer function in the vicinity of the acoustic axis. It can be concluded then that the hydrophone range employed was sufficient for determining the far-field transfer function on the major lobe. It is also apparent that precise measurements for angles further removed from the acoustic axis require a greater hydrophone range. In general, the monitor hydrophone should be placed at the greatest practical range during calibration procedures. The widely used rule-of-thumb range criteria of ℓ^2/λ, where ℓ is the maximum dimension of the transducer, is not sufficient for obtaining precise directivity patterns. It is evident that, in cases where the depth of nulls is of interest, as in receiving arrays in which a null is steered to a noise spoke, careful attention must be given to the ranges at which measurements are made. This also points out a problem in null steering when a noise source is at close range.

Having satisfied the necessary conditions of adequate range and positional stability for the monitor hydrophone, the fidelity of an acoustic source can be determined by measurement of the transfer function. It is a way of completely specifying the input-output relations for a system. The practical importance of the transfer function is that it can be determined for a linear, time-invariant system of any degree of complexity by a set of steady-state measurements using sine waves. The techniques and equipment needed for such measurements are readily available.

There is some uncertainty to what extent high-power acoustic sources can be considered linear and time-invariant systems. It is known that such systems are not strictly linear over a large dynamic range. There is reason to believe they are not time-invariant. If a transfer function for such a source is measured using sine waves, this transfer function may not determine the input-output relations for all types of inputs. For this reason, it was decided to measure the transfer function of the ARTEMIS source using two different types of inputs. First, the transfer function was measured using sine-wave inputs. Second, the transfer function was measured by spectral analysis techniques using a pseudorandom signal as the input. A comparison of these two types of transfer-function measurements answers in part the question of the adequacy of sine-wave measurements for the ARTEMIS source.

Sine-Wave Measurements of the Transfer Function for the ARTEMIS Source

The ARTEMIS source is represented by the block diagram (Fig. 12). The input to the system is the input voltage to the console of the power amplifier. The output

of the source is the acoustic pressure measured by a hydrophone held fixed about 190 feet from the center of the face of the transducer array. The transfer function $H(\omega)$ is the ratio as a function of frequency of the complex phasors $P(\omega)$ and $V(\omega)$ of the acoustic pressure and input voltage, respectively.

$$H(\omega) = \frac{P(\omega)}{V(\omega)} . \tag{1}$$

In the transfer function $H(\omega)$, there is a factor representing a phase lag which is proportional to frequency. This corresponds to distortionless transmission due to a time delay. Part of this phase lag is due to the time delay, τ_p (time required for the propagation of a plane wave from the center of the array to the hydrophone). This represents a factor in the transfer function of

$$e^{-j\omega\tau_p} .$$

The transfer function can now be written as

$$H(\omega) = H_o(\omega)e^{-j\omega\tau_p} , \tag{2}$$

where $H_o(\omega)$ is interpreted as the transfer function to zero range.

The method of measurement of $H_o(\omega)$ is illustrated in Fig. 13. An oscillator produces a sine-wave voltage waveform of frequency f, which is the input to the source. A zero-crossing detector detects a zero crossing of this voltage which produces a pulse which is delayed for a time, τ_p, and then starts a counter. A zero crossing of the acoustic pressure is detected, producing a pulse which stops the counter. The counter has been counting a frequency 360 times f, so the count is the phase of $H_o(\omega)$ with a resolution of ±1 degree. The amplitude of the input voltage and acoustic pressure was measured using an average reading vacuum-tube voltmeter. Measurements were completed at five-hertz increments of frequency from 350 to 450 hertz.

Figure 14 illustrates the resulting transfer-function amplitude and phase for the ARTEMIS source. The data are illustrated for three values of current: 8, 20, and 40 amperes. For any one current value, the amplitude displays approximately

a two-decibel change over the frequency band, whereas the phase is very nearly linear and is very nearly free of distortion. The linear phase results from time shifts in the amplifier and transducer plus any propagation delay which has not been completely subtracted out. A linear phase shift, however, does not represent distortion. Considerable nonlinearity is evidenced by the divergence of the data between 8 and 80 amperes. The nonlinearity, however, was not evidenced in spectral measurements in which the harmonic content of the acoustic signal was found to be more than 40 decibels below the fundamental when the array was driven at 420 hertz. Also, it will be shown that, when broad-band signals were used, the measured transfer-function phase was identical with the phase characteristics measured with a continuous-wave input having an input current equal to the average current for the broadband signal. The nonlinearity, therefore, appears to be a function of average rather than instantaneous power and does not result in signal distortion.

The amplitude and phase characteristics of the source are plotted in Fig. 15 as a function of hydrophone angle relative to the acoustic axis. For comparison, the computed near-field characteristics are shown as dotted curves. In these plots, the amplitudes and the computed phase have been referenced to zero on the acoustic axis. The close agreement between computed and measured values indicates that the real array has a response which closely resembles an ideal, uniform-velocity piston.

Measurement of the Transfer Function Using Pseudorandom-Sequence Signals

Signal Characteristics - A maximal length linear shift register sequence of ones and zeros was used to modulate a 400 hertz square wave. An output of one from the shift register does not change the carrier. An output of zero is equivalent to multiplying the carrier by -1 or changing its phase 180 degrees. This binary waveform was then passed through a bandpass filter, United Transformer Corp. type CF-765A, having a center frequency of 400 hertz and pass band from 345-455 hertz. The output of the filter was the signal used as the input of the source. This signal is referred to as phase modulation, although it might equally well be called suppressed-carrier amplitude modulation. The signal has a low peak-to-rms ratio.

Two pseudorandom-sequence signals were used in the transfer-function measurements. Both had the same duration. The difference was the shift-rate

and feedback connections used in the shift-register generator. Different shift rates were used to change the bandwidth of the signal. The power spectrum of the signal is roughly a

$$\left(\frac{\sin X}{X}\right)^2$$

shape centered about the carrier frequency. The first nulls in the spectrum occur at frequencies of the carrier plus or minus the shift rate. Table 3 gives a description of the two signals.

TABLE 3

Carrier frequency	400 Hz	400 Hz
Duration	41 sec	41 sec
Shift rate	100 Hz	50 Hz
Shift-register length	12 bits	11 bits
Frequency of first nulls	300, 500 Hz	350, 450 Hz
Shift-register sequence[6]	Degree 12	Degree 11
	Code 1:10123F	Code 167:52056

[6] Error Correcting Codes, (W. W. Peterson), The MIT Press, 1961

Method of Measurement - The cross-power spectrum between two signals having Fourier spectrums $X(\omega)$ and $Y(\omega)$ is defined as

$$S_{xy}(\omega) = X(\omega)Y(\omega)^*, \tag{3}$$

where * represents complex conjugation. The power spectrum of $X(\omega)$ is defined as

$$S_{xx}(\omega) = X(\omega)X(\omega)^* = |X(\omega)|^2. \tag{4}$$

The spectrum $X(\omega)$ is to be considered as the input to a linear time-invariant system and $Y(\omega)$ the output of the system. The system has a transfer function $H(\omega)$, so

$$Y(\omega) = H(\omega)X(\omega), \tag{5}$$

and substituting this into definition of cross-power spectrum gives

$$S_{xy}(\omega) = X(\omega)H(\omega)^*X(\omega)^* = H(\omega)^*S_{xx}(\omega). \tag{6}$$

From Eq. (6), the real and imaginary components of the transfer function are

$$\mathrm{Re}[H(\omega)] = \frac{\mathrm{Re}[S_{xy}(\omega)]}{S_{xx}(\omega)} , \tag{7}$$

$$\mathrm{Im}[H(\omega)] = \frac{-\mathrm{Im}[S_{xy}(\omega)]}{S_{xx}(\omega)} . \tag{8}$$

To determine the transfer function $H(\omega)$ of the system, it is necessary to measure the real and imaginary components of the cross-power spectrum between input and output $S_{xy}(\omega)$ and the power spectrum of the input $S_{xx}(\omega)$.

The cross-power and power spectrum were measured by the analyzer shown as a block diagram in Fig. 16. Each block represents electronic circuitry which does the analog of such operations as amplification, multiplication, filtering, adding, and integrating. A measurement of cross-power or power spectrum using this analyzer refers to an average over a narrow band of frequencies. The measured cross-power spectrum about frequency ω_o (angular frequency) is denoted by $S'_{xy}(\omega_o)$ and is defined as

$$S'_{xy}(\omega_o) = \frac{1}{B}\int_{\omega_o - \frac{B}{2}}^{\omega_o + \frac{B}{2}} S_{xy}(\omega)d\omega = \frac{1}{B}\int_{\omega_o - \frac{B}{2}}^{\omega_o + \frac{B}{2}} X(\omega)Y(\omega)^*d\omega \tag{9}$$

where B is the analyzing bandwidth, with the prime indicating an average over the band of frequencies between $\omega_o - \frac{B}{2}$ and $\omega_o + \frac{B}{2}$. Similarly, a measurement of power spectrum $S'_{xx}(\omega_o)$ is

$$S'_{xx}(\omega_o) = \frac{1}{B}\int_{\omega_o - \frac{B}{2}}^{\omega_o + \frac{B}{2}} S_{xx}(\omega)d\omega . \tag{10}$$

Substituting into Eq. (9) for $S_{xy}(\omega)$ from Eq. (6) gives

$$S'_{xy}(\omega_o) = \frac{1}{B}\int_{\omega_o - \frac{B}{2}}^{\omega_o + \frac{B}{2}} H(\omega)^* S_{xx}(\omega)d\omega . \tag{11}$$

In order that the transfer-function measurements have a definite meaning, it must be assumed $H(\omega)^*$ is constant for the ω interval of the integration so that we can write

$$S'_{xy}(\omega_o) = \frac{1}{B}H(\omega_o)^*\int_{\omega_o - \frac{B}{2}}^{\omega_o + \frac{B}{2}} S_{xx}(\omega)d\omega , \tag{12}$$

from which

$$S'_{xy}(\omega_o) = H(\omega_o)^* S'_{xx}(\omega_o). \tag{13}$$

The transfer function is then given by

$$Re[H(\omega_o)] = \frac{Re[S'_{xy}(\omega_o)]}{S'_{xx}(\omega_o)} , \tag{14}$$

$$Im[H(\omega_o)] = \frac{-Im[S'_{xy}(\omega_o)]}{S'_{xx}(\omega_o)} , \tag{15}$$

where $Re[S'_{xy}(\omega_o)]$, $Im[S'_{xy}(\omega_o)]$, and $S'_{xx}(\omega_o)$ are the quantities to be measured by the analyzer.

Equations (9) and (10) indicate spectrum measurements are made using bandpass filters of bandwidth B. The analyzer shown in Fig. 16 actually uses low-pass filters which pass frequency components between $-B/2$ and $+B/2$. It will now be shown that the analyzer using low-pass filters measures

the quantities $S'_{xy}(\omega_o)$ and $S'_{xx}(\omega_o)$. The gains associated with the various blocks in the analyzer can be ignored. Since the transfer function is a ratio of two measurements using the same equipment, the gains are eliminated from the final result. It is necessary to have equal gains in various parallel channels and this is easily obtained.

The Fourier spectrum of the input $X(\omega)$ is broken up into a positive frequency part $X_1(\omega)$ and a negative frequency part $X_2(\omega)$.

$$X(\omega) = X_1(\omega) + X_2(\omega), \tag{16}$$

where

$$X_1(\omega) = X(\omega) \quad \omega > 0$$
$$X_1(\omega) = 0 \quad \omega < 0$$

and

$$X_2(\omega) = 0 \quad \omega > 0$$
$$X_2(\omega) = X(\omega) \quad \omega < 0.$$

A similar definition is used for $Y(\omega)$. Referring to Fig. 16, the input time function $x(t)$, corresponding to $X(\omega)$, is multiplied by

$$\cos\omega_o t = \frac{e^{j\omega_o t} + e^{-j\omega_o t}}{2}$$

in the block labeled modulator. The resultant time function is passed through a low-pass filter which passes angular frequency component within $\pm B/2$ of zero frequency. Using the relation for complex modulation of a time function, the spectrum of the output of the low-pass filter $X_p(\omega)$ is

$$X_p(\omega) = \frac{X_2(\omega-\omega_o) + X_1(\omega+\omega_o)}{2} \quad \text{for } -\frac{B}{2} < \omega < \frac{B}{2}, \text{ and} \tag{17}$$

$$X_p(\omega) = 0 \text{ elsewhere.}$$

The input x(t) is also multiplied by

$$\sin\omega_o t = \frac{e^{j\omega_o t} - e^{-j\omega_o t}}{2j}$$

and low-pass filtered, resulting in a waveform with spectrum $X_q(\omega)$.

$$X_q(\omega) = \frac{X_2(\omega - \omega_o) - X_1(\omega + \omega_o)}{2j} \quad \text{for } -\frac{B}{2} < \omega < \frac{B}{2} \text{ and} \tag{18}$$

$$X_q(\omega) = 0 \quad \text{elsewhere.}$$

Treating the spectrum $Y(\omega)$ the same way gives

$$Y_p(\omega) = \frac{Y_2(\omega - \omega_o) + Y_1(\omega + \omega_o)}{2} \quad \text{for } -\frac{B}{2} < \omega < \frac{B}{2}, \text{ and} \tag{19}$$

$$Y_q(\omega) = \frac{Y_2(\omega - \omega_o) - Y_1(\omega + \omega_o)}{2j} \quad \text{for } -\frac{B}{2} < \omega < \frac{B}{2}. \tag{20}$$

Solving Eqs. (17) and (18) for $X_1(\omega + \omega_o)$ and (19) and (20) for $Y_2(\omega + \omega_o)$ gives

$$X_1(\omega + \omega_o) = X_p(\omega) - jX_q(\omega) \tag{21}$$

$$Y_1(\omega + \omega_o) = Y_p(\omega) - jY_q(\omega) \tag{22}$$

for $-\frac{B}{2} < \omega < \frac{B}{2}$.

Returning to the definition of measured cross-power spectrum (Eq. 9).

$$S'_{xy}(\omega_o) = \frac{1}{B}\int_{\omega_o - \frac{B}{2}}^{\omega_o + \frac{B}{2}} X(\omega)Y(\omega)^* d\omega,$$ and, since the integration is over positive frequencies,

$$S'_{xy}(\omega_o) = \frac{1}{B}\int_{\omega_o - \frac{B}{2}}^{\omega_o + \frac{B}{2}} X_1(\omega)Y_1(\omega)^* d\omega . \tag{23}$$

Making change of variables gives

$$S'_{xy}(\omega_o) = \frac{1}{B}\int_{-B/2}^{B/2} X_1(\omega + \omega_o)Y_1(\omega + \omega_o)^* d\omega . \tag{24}$$

Substituting into Eq. (24), $X_1(\omega + \omega_o)$ and $Y_1(\omega + \omega_o)^*$ from Eqs. (21) and (22) gives

$$S'_{xy}(\omega_o) = \int_{-B/2}^{B/2} [X_p(\omega) - [X_q(\omega)]\ [Y_p(\omega) - [Y_q(\omega)]^* d\omega . \tag{25}$$

Expanding and rearranging terms, this becomes

$$S'_{xy}(\omega_o) = \int_{-B/2}^{B/2} [X_p(\omega)Y_p(\omega)^* + X_q(\omega)^*] d\omega$$

$$+ i\int_{-B/2}^{B/2} [X_p(\omega)Y_q(\omega)^* - X_q(\omega)Y_p(\omega)^*] d\omega . \tag{26}$$

The values of both definite integrals in Eq. (26) are real. This follows from the fact

$$X_p(\omega) = X_p(-\omega)^*, \tag{27}$$

$$X_q(\omega) = X_q(-\omega)^*,$$

$$X_p(\omega) = Y_p(-\omega)^*, \text{ and}$$

$$Y_q(\omega) = Y_q(-\omega)^*,$$

which can be shown by manipulation or noting that they represent Fourier spectrums of real time functions. Therefore, the first integral in Eq. (26) represents $Re[S'_{xy}(\omega_o)]$ and the second integral $Im[S'_{xy}(\omega_o)]$. The analyzer performs the integration over frequencies indicated by Eq. (26) by multiplying the corresponding time functions and integrating. If $f_1(t)$ and $f_2(t)$ are real time functions and $F_1(\omega)$ and $F_2(\omega)$ are their Fourier transforms,

$$\int_{-\infty}^{\infty} f_1(t)f_2(t)dt = \int_{-\infty}^{\infty} F_1(\omega)F_2(\omega)^* d\omega . \tag{28}$$

The final value of the output of the integrators is, respectively, $Re[S'_{xy}(\omega_o)]$ and $Im[S'_{xy}(\omega_o)]$. To measure the power spectrum of $X(\omega)$ using the same analyzer, put $Y(\omega) = X(\omega)$.

Measurement of the transfer function of the ARTEMIS array using the cross-power spectrum analyzer is shown in Fig. 17. The generator output is bandpass filtered to 345–455 hertz, producing a signal with spectrum $V(\omega)$ used as the input to the source. The generator output is precisely delayed by a time τ_p and bandpass filtered, producing a signal with spectrum $V(\omega)e^{-j\omega\tau_p}$. This signal is used as the reference input to the analyzer or what was called $X(\omega)$ in the previous discussion. The acoustic pressure at the hydrophone $P(\omega)$ is the $Y(\omega)$ input to the analyzer. The analyzer measures the transfer function of the source $H_o(\omega_o)$ as defined in Eq. (4). $H_o(\omega_o)$ is the transfer function of the source at angular frequency ω_o after the factor $e^{-j\omega_o\tau}$ due to pure time delay has been eliminated. The elimination of $e^{-j\omega_o\tau}$ factor by introducing a delay reference into the analyzer is an essential part of the measurement. The delay τ_p causes a phase shift of about 14 degrees per hertz frequency change. If this phase shift is not eliminated, it is not possible to assume the measured transfer function is constant over the analyzing bandwidth. The analyzing bandwidth used in the measurements was four hertz. Measurements were made at frequencies four hertz apart from 350 to 450 hertz.

Another type of measurement was made to check the coherence of the ARTEMIS source. Because of the large time-bandwidth product of the measurements (about 200), the cross-power spectrum measurement ignores incoherent energy. By measuring both the input and output power spectrum $S'_{xx}(\omega)$ and $S'_{yy}(\omega)$, it is possible to define a coherence ratio for the source.

$$\gamma(\omega_o) = \frac{|S'_{xy}(\omega_o)|}{\sqrt{S'_{xx}(\omega_o) \quad S'_{yy}(\omega_o)}} . \tag{29}$$

This ratio is equivalent to the normalized cross-correlation for the band of frequencies

$$\omega_o - \frac{B}{2} < \omega < \omega_o + \frac{B}{2}.$$

If the system is fully coherent, $\gamma(\omega_o)$ should equal unity at all frequencies. Values less than unity are interpreted in terms of loss of coherence.

Results - The transfer-function phase data for 8 and 80 amperes sine wave shown in Fig. 14 is reproduced to an expanded scale in Fig. 18, along with the phase data measured with a pseudorandom sequence. The average value of the rms current for the pseudorandom sequence signal was 80 amperes. The signal had a shift rate of 100 hertz. The excellent agreement between the broadband and continuous-wave data at 80 amperes indicates that the phase nonlinearity of the source is a function of average rather than instantaneous current since the individual frequency components of the pseudorandom sequence signal have amplitudes which are very small compared to 80 amperes. It would not be expected then that the nonlinearity of the source would degrade its performance with broadband signals.

The magnitude and phase characteristics of the transfer function at angles of 0°, 7.5°, and 20° relative to the acoustic axis are plotted in Figs. 19 and 20. The 7.5° position is below the acoustic axis on one side of the major lobe and the 20° position is below the acoustic axis on the first minor lobe. The solid lines were plotted from data of the 100 hertz shift-rate sequence

and the dotted curves with circled points from the 50-hertz shift-rate sequence. The phase data has been referenced to zero degrees at 400 hertz by subtracting a linear phase shift. The phase and amplitude distortion is small at all angles investigated, and no significant difference is observed between the two types of modulated waveforms.

The coherence ratios are not illustrated since they have no significant deviation from unity. For all frequencies within the operating band and for all angles with respect to the acoustic axis from 0 to -20°, the coherence ratios computed from the measured data fell within the range of 0.99 to 1.01. Since the accuracy of the spectral analysis equipment is considered to be ±2 percent, the coherence ratios are unity within the accuracy of measurement.

Cross-Correlation Function Measurements

Figure 21 shows the method of measurement of the cross-correlation function between the input and output of the source. The input was a pseudorandom-sequence signal generated by the digital generator previously described. The output of the digital generator was sampled at a rate of 800 times a second synchronous with its shift pulses. These samples were entered into one end of a 64-bit shift register. By picking off the signal along the stages of the shift register, a time delay τ, in increments of 1.25 milliseconds, from 0 to 80 milliseconds was obtained. By varying the sampling of the output of the generator relative to its clock from 0 to 1.25 milliseconds, any delay from 0 to 80 milliseconds can be obtained. The output of the generator and shift register were filtered by a matched pair of bandpass filters (United Transformer Corp. type CF-765A) to obtain the signal $v(t)$ into the source and a reference signal $v(t-\tau)$ used in the cross-correlation.

As shown in Fig. 21, the acoustic pressure $p(t)$ was multiplied by $v(t-\tau)$ and integrated for the 41-second duration of the signal. The final value of the integrator was held and read out using a digital voltmeter.

Aside from a constant factor which represents the various gains in the measurement system, the final value of the integrator output is the cross-correlation $R(\tau)$ between the input and output of the source.

$$R(\tau) = \int_0^T p(t)v(t-\tau)dt. \tag{30}$$

To reduce the time required to complete the measurements, it was decided to use only values of τ which correspond to the peaks (positive or negative) of the fine structure of the cross-correlation function. Peaks occur for values of τ 1.25 milliseconds apart; that is, half the period of the 400 hertz carrier. By varying the sampling of the generator output over 1.25 milliseconds relative to the carrier, a few measurements would locate a peak in the fine structure. After that was found, other peaks could be obtained by tapping off the signal along the shift register.

Since there was a pure time delay of about 40 milliseconds in the source and a delay of up to 80 milliseconds was available, it was possible to obtain values of the cross-correlation function 40 milliseconds on either side of the peak of its envelope. This range of τ determines the cross-correlation through its main lobe out past the first side lobes.

The normalized cross-correlation function is defined as

$$\rho(\tau) = \frac{\int_0^T p(t)v(t-\tau)dt}{\left[\int_0^T p(t)^2 dt \int_0^T v(t)^2 dt\right]^{1/2}}. \tag{31}$$

The integrals of $p(t)^2$ and $v(t)^2$ were obtained by the same multiplier-integrator combination used in the cross-correlation function measurements. It is then possible to compute $\rho(\tau)$.

The correlograms obtained between the input signal and the hydrophone outputs confirm that negligible decorrelation is produced by the ARTEMIS source. Figure 22 illustrates the normalized cross-correlations obtained with 50- and 100-hertz shift-rate sequences. There are no measurable differences between these curves and plots of the normalized autocorrelation functions of the corresponding input signals. Although these plots were made from data obtained with a hydrophone on the acoustic axis, they are identical with correlations obtained at angles up to 22 degrees below the axis. It can be concluded that this source generates an acoustic field which is a replica of the input time function with negligible distortion.

SUMMARY

The potential gain in sonar performance to be obtained by maximizing signal power justifies increased effort addressed to this problem. Adequate techniques are needed to

1. Determine the factors which limit the allowable input power to acoustic sources,

2. Test nondestructively the power limitation in existing transducers when driven with useful types of modulated signals,

3. Establish design criteria for optimizing power capability of sources to be used with specific types of signals, and

4. Test transducers for phase and amplitude distortion.

Acoustic sources having dimensions which are large compared to the sound wavelength in water are inherently subject to large variations in acoustic loading over the radiating face. Variations in loading resulting from acoustic interactions are both spatial and temporal, being related to the physical geometry of the source and the time function of the signal modulation. If the range of values over which the real and reactive parts of the acoustic load can vary is determined for a particular array, and, if all elements of the array can be assumed to be electrically and mechanically identical, then the power capability of the array can be predicted from an analysis of a single element. The transient response of the power-limiting factors within a transducer element are difficult to predict analytically or measure experimentally. These factors, which might be in the form of mechanical or electrical stress, temperature, or dimensional tolerances, are usually peak limited. Each factor has an upper limit which, if exceeded, results in nonlinear operation or failure of the element. Which factor, however, actually limits the power input to the element depends upon external conditions such as acoustic load, excitation frequency, or driver output impedance. The limiting factor under one set of conditions may be replaced by another factor under a different set of conditions.

Analog modeling is an attractive technique for transient analysis of the power-limiting factors in that all dynamic quantities are represented as voltages or currents and thus are readily accessible for measurement and

external variables such as acoustic load are easily controllable. This method is limited, however, by the ability to faithfully represent a mechanical system with all its degrees of freedom by an electrical circuit. In this method, as in any other, it is necessary to be able to predict the range over which the components of the acoustic load can vary in operation. No adequate method is presently available to do this.

The increased emphasis on coherent signal-processing techniques has brought about a need for more sophisticated transducer test procedures than have been conventionally required. Techniques used in obtaining the transfer function, coherence ratios, and cross-correlation between the electrical input and acoustic output of the ARTEMIS acoustic source serve as an example of the types of instrumentation required.

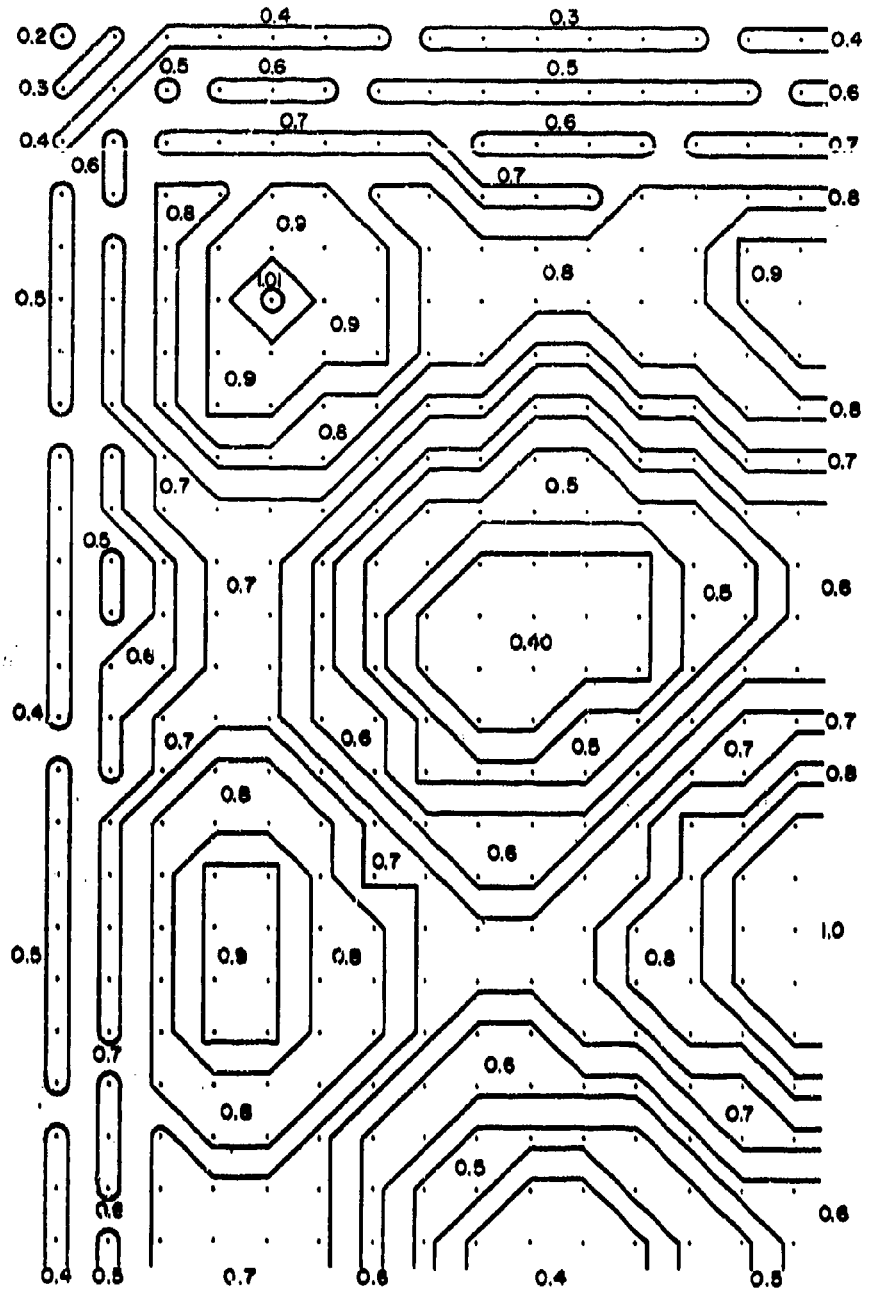

AVE = 0.696

Fig. 1 - Real part of radiation load for one quadrant of a 2-1/2 by 4 wavelength uniform velocity piston

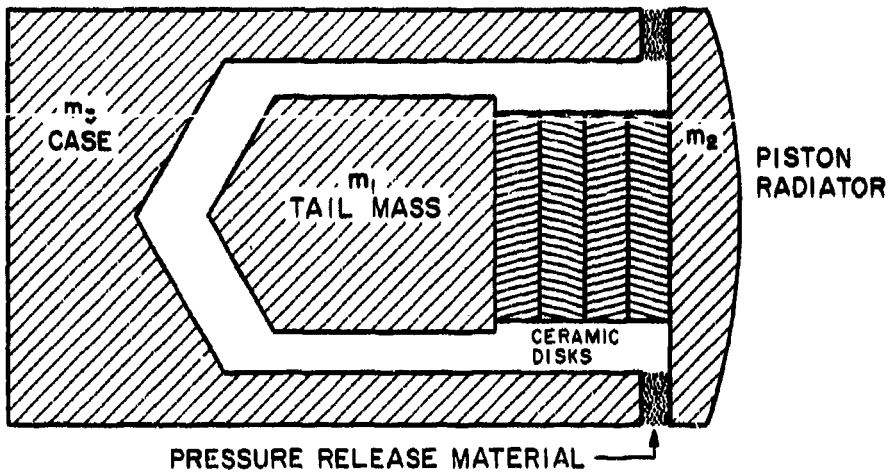

Fig. 2 - Basic configuration of an illustrative ceramic element

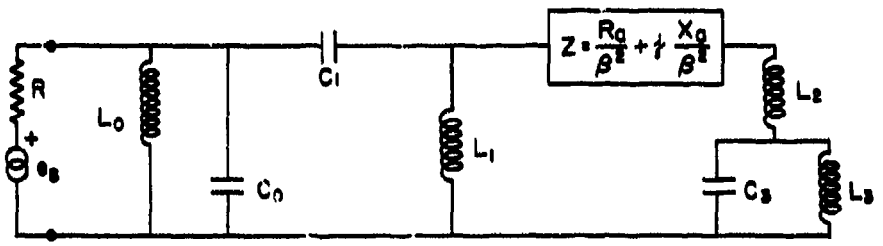

L_0 = ACTUAL SHUNT TUNING INDUCTANCE IN HENRIES
C_0 = ACTUAL SHUNT CAPACITANCE OF CERAMIC STACK IN FARADS
C_1 = EQUIVALENT CAPACITANCE DUE TO CERAMIC STIFFNESS
C_3 = " " " " PRESSURE RELEASE MAT'L
L_1 = EQUIVALENT INDUCTANCE DUE TO MASS m_1
L_2 = " " " " " m_2
L_3 = " " " " " m_3

$C_1 = \beta^2$ $\qquad$ β = ELECTROMECHANICAL TURNS RATIO

$C_3 = \beta^2/k_3$

k_1 & k_2 ARE STIFFNESS COEFFICIENTS FOR THE CERAMIC AND PRESSURE RELEASE MAT'L

$L_1 = m_1/\beta^2$

$L_2 = m_2/\beta^2$ $\qquad$ $R_a + j X_a$ = ACOUSTIC RADIATION IMPEDANCE

$L_3 = m_3/\beta^2$

Fig. 3 - Equivalent circuit of the element shown in Figure 2

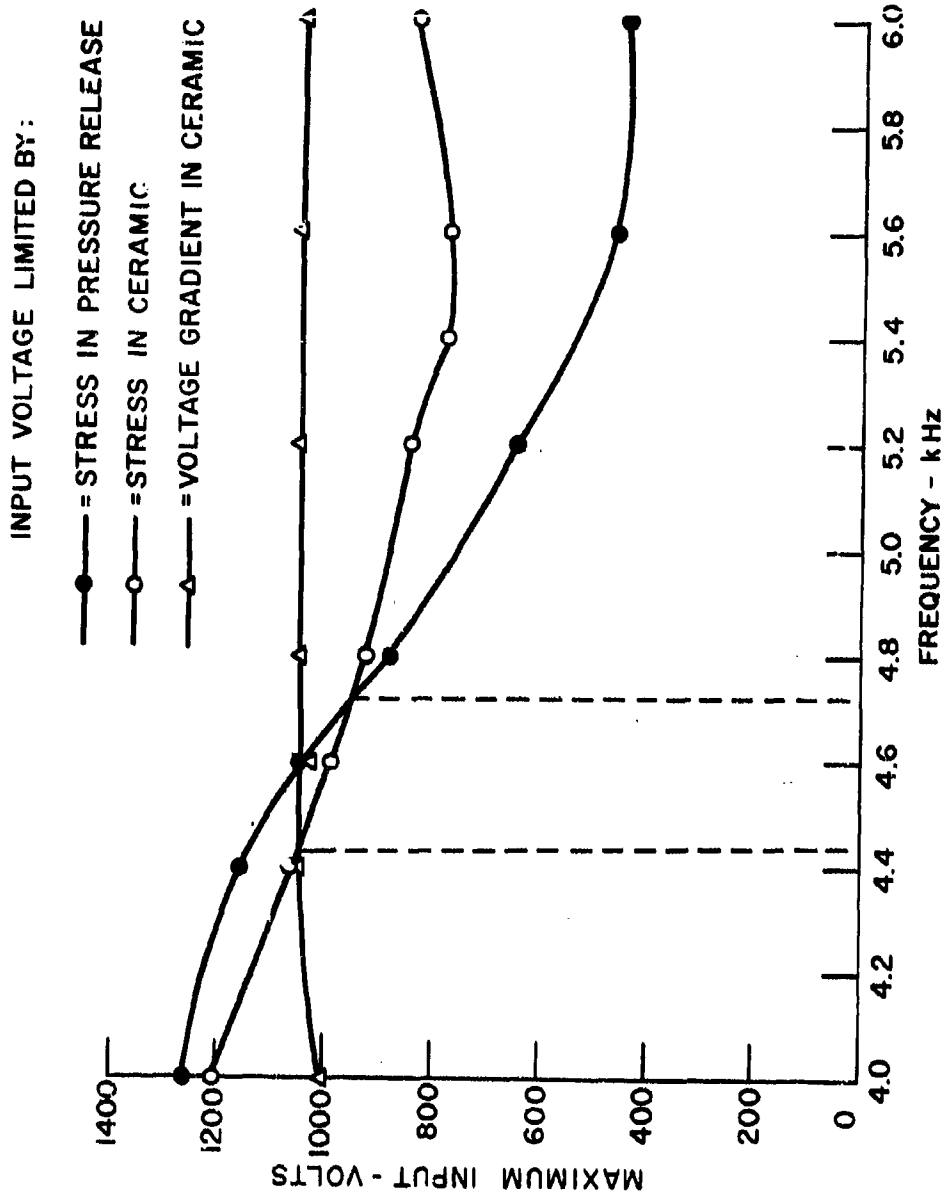

Fig. 4 - Maximum allowable voltage input to the ceramic element shown in Figure 2 for three limiting factors

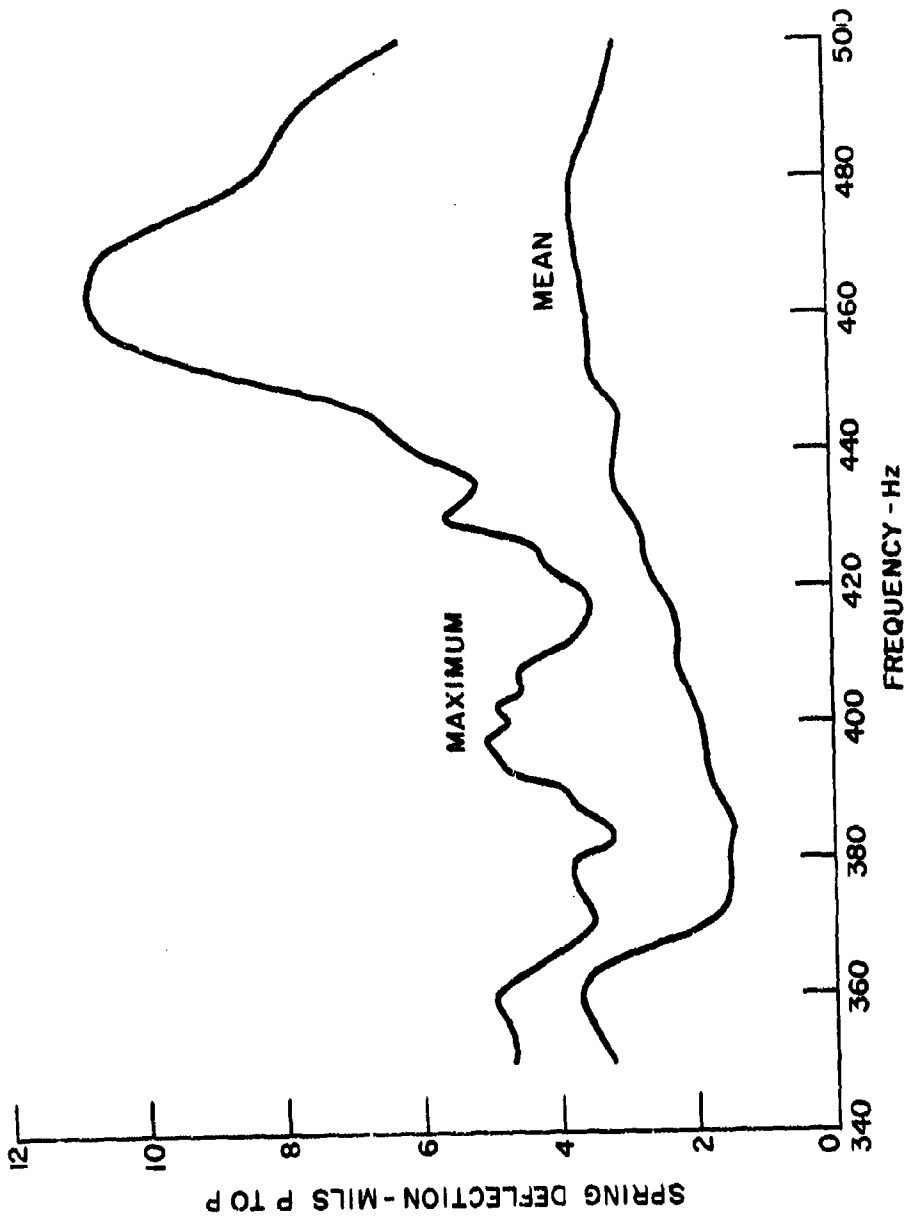

Fig. 5 - Mean and maximum observed spring deflections in the Artemis source for steady state drive

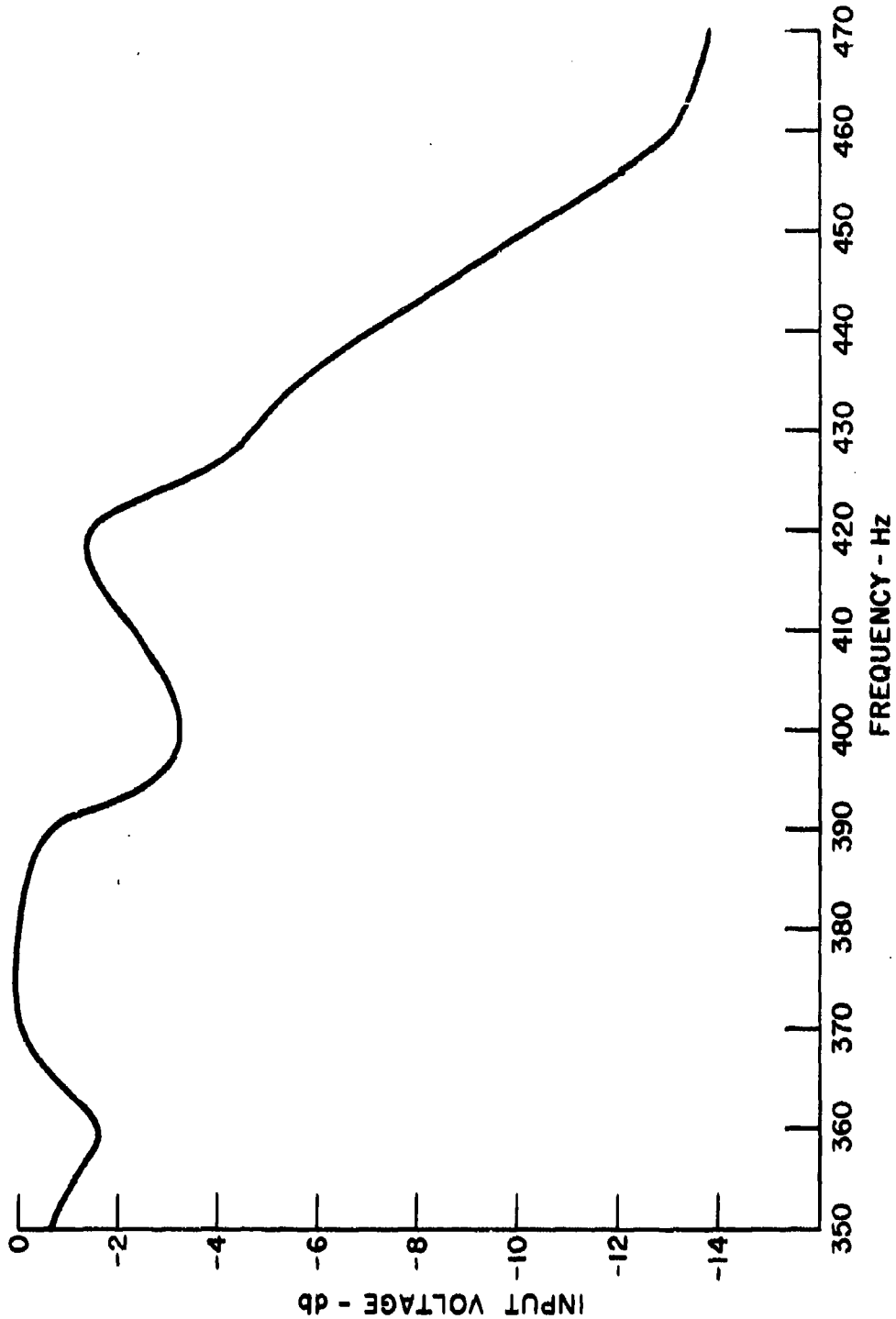

Fig. 6 - Relative permissible voltage input to the Artemis source as determined by spring deflection limitation

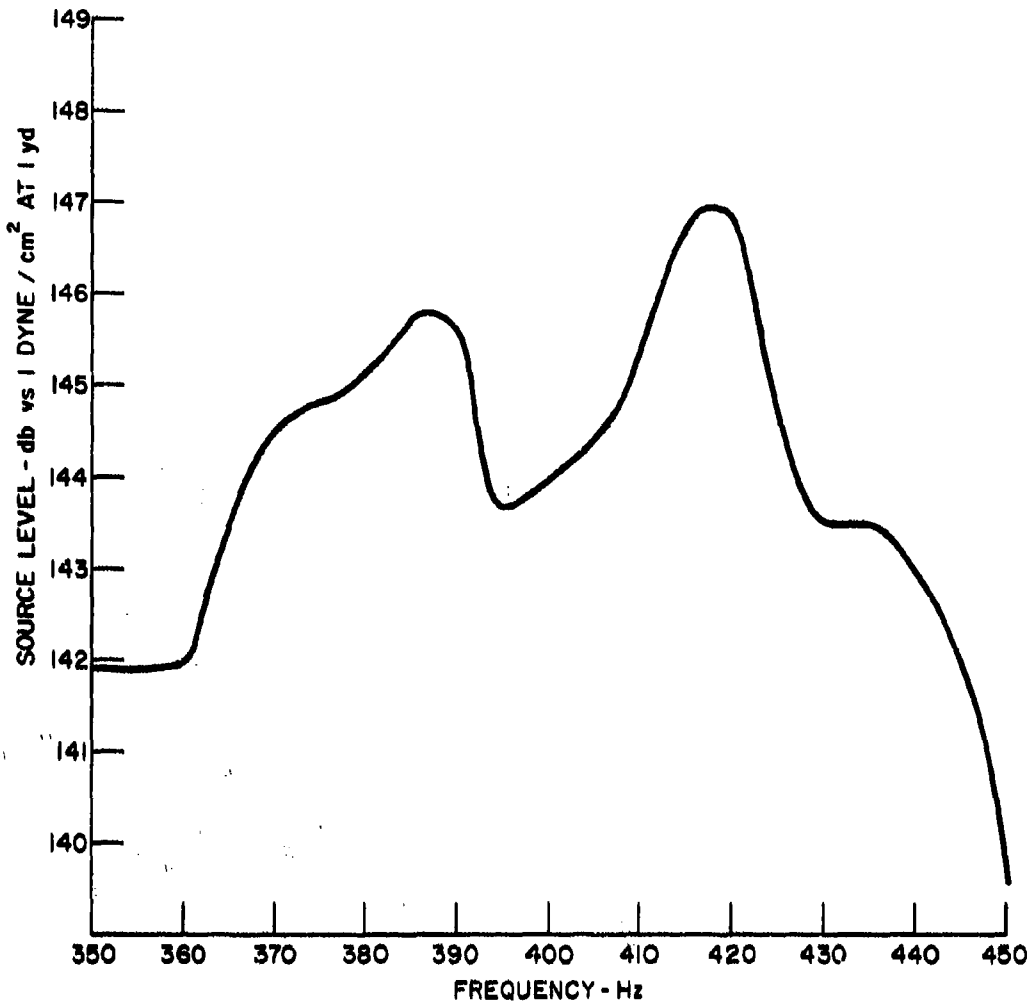

Fig. 7 - Maximum safe source level for the Artemis source with sine wave excitation

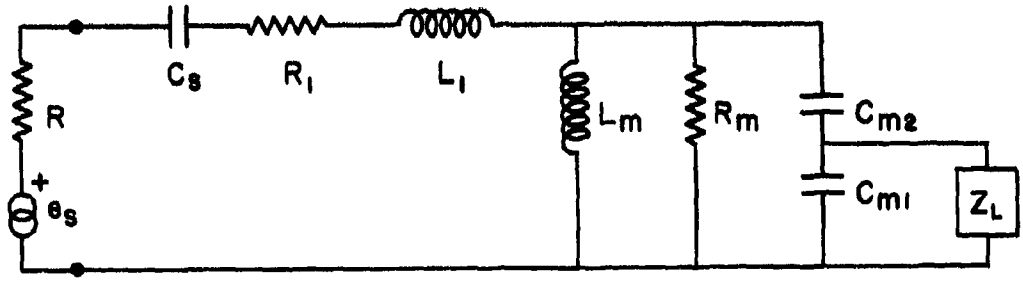

Z_L = EQUIVALENT IMPEDANCE DUE TO THE ACOUSTIC RADIATION IMPEDANCE

C_{m1} = EQUIVALENT CAPACITANCE DUE TO OUTER MASS m1

C_{m2} = EQUIVALENT CAPACITANCE DUE TO INNER MASS m2

R_m = EQUIVALENT DISSIPATION ELEMENT

L_m = EQUIVALENT INDUCTANCE DUE TO SPRING STIFFNESS

R_1 = ACTUAL WINDING RESISTANCE

L_1 = ACTUAL WINDING INDUCTANCE

C_s = SIGNAL COUPLING CAPACITOR

R = SOURCE RESISTANCE

Fig. 8 - Equivalent circuit of the Artemis transducer element

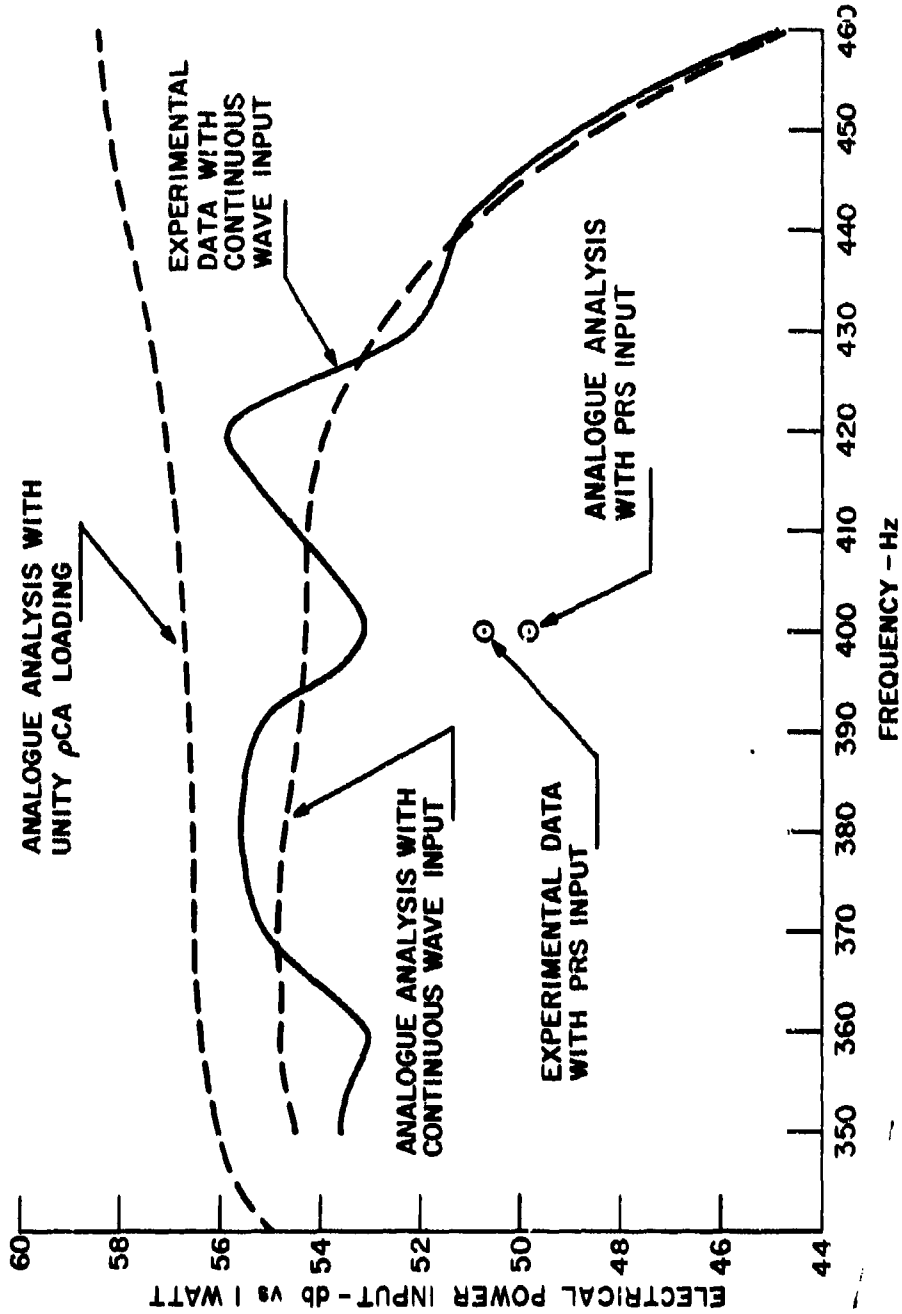

Fig. 9 - Maximum allowable power input to the Artemis source as determined experimentally and by analogue circuit analysis

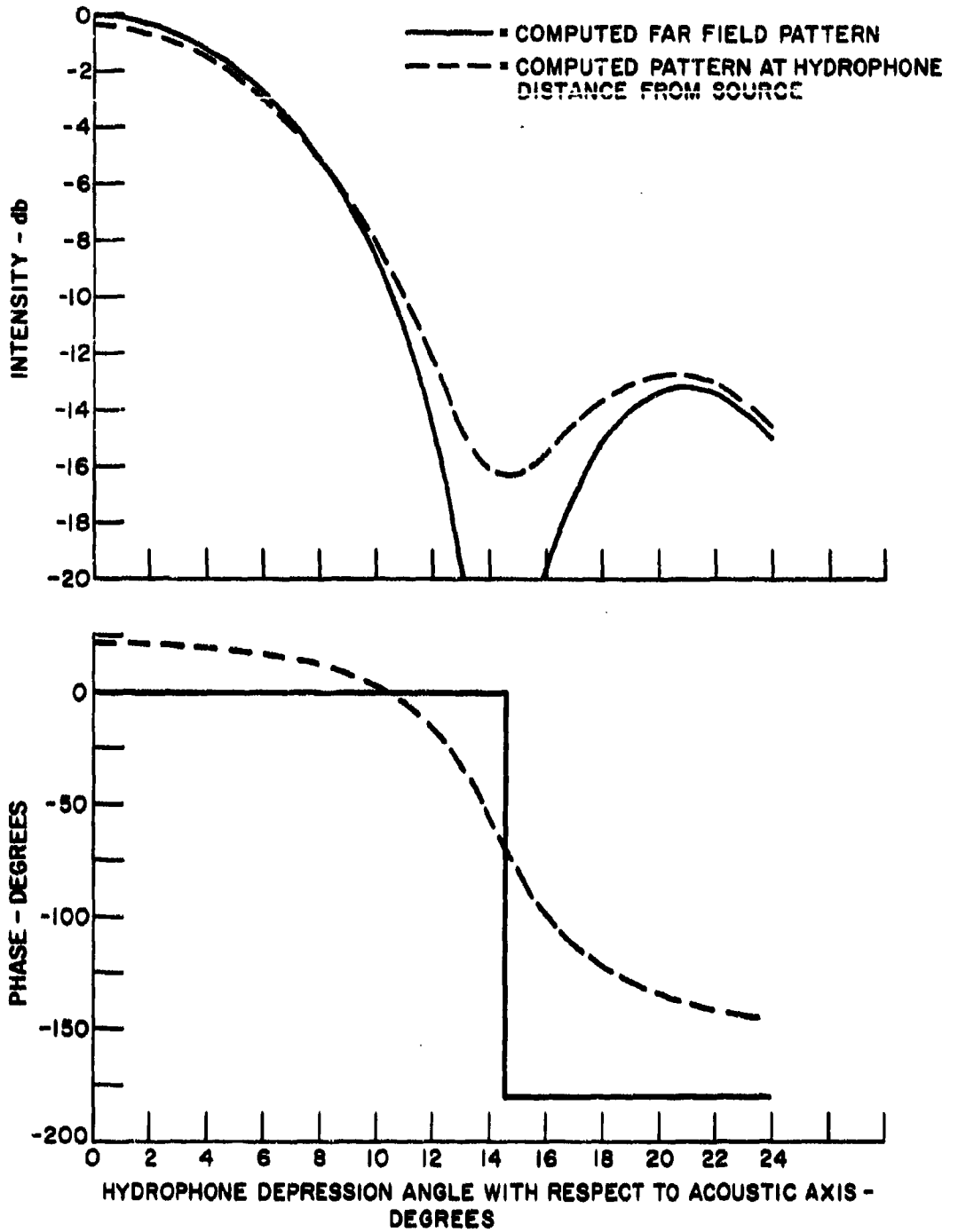

Fig. 10 - Computed 400 hertz directivity pattern for a piston having the dimensions of the Artemis source

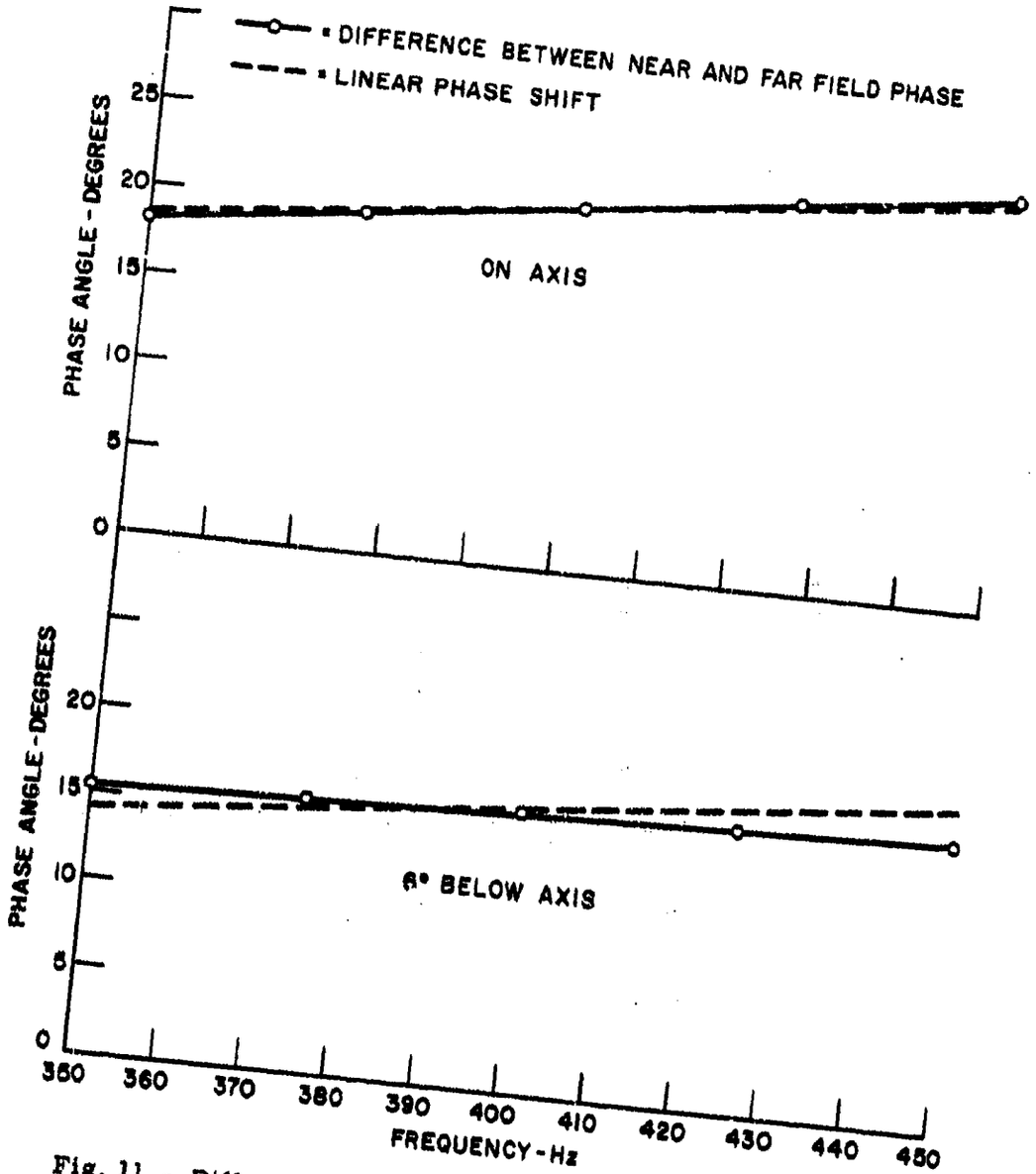

Fig. 11 - Difference between computed near-field phase at hydrophone distance and equivalent far-field phase compared with linear phase shifts

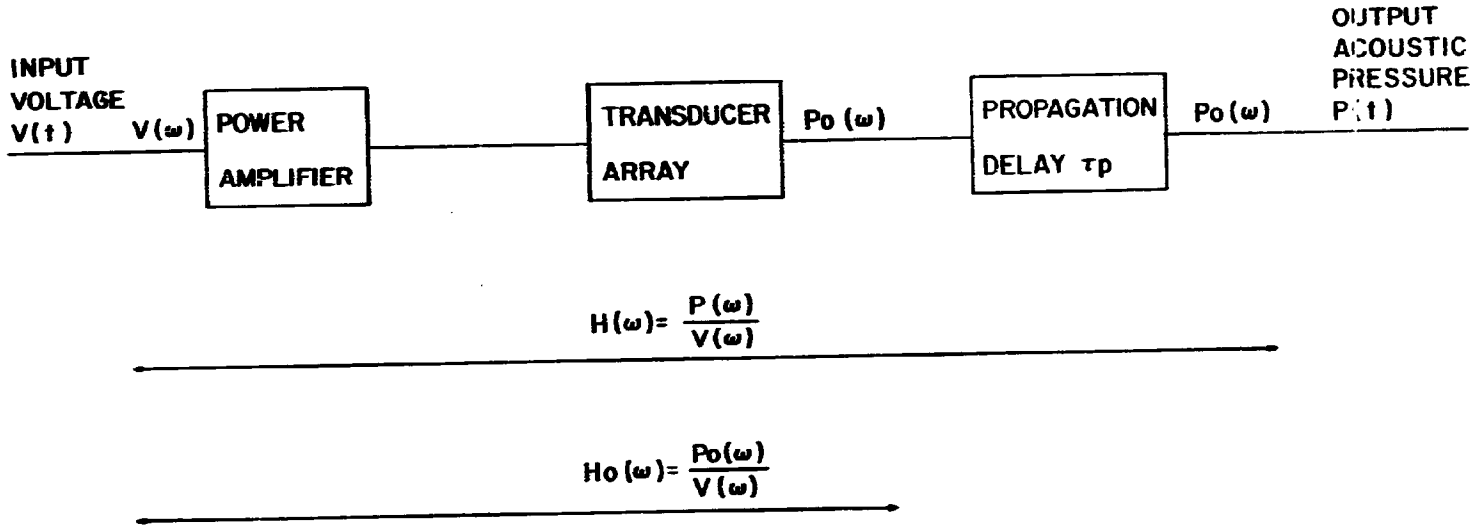

$$H(\omega) = \frac{P(\omega)}{V(\omega)} = \frac{e^{-j\omega\tau p}\, Po(\omega)}{V(\omega)} = e^{-j\omega\tau p}\; Ho(\omega)$$

Fig. 12 - Block diagram of the Artemis source

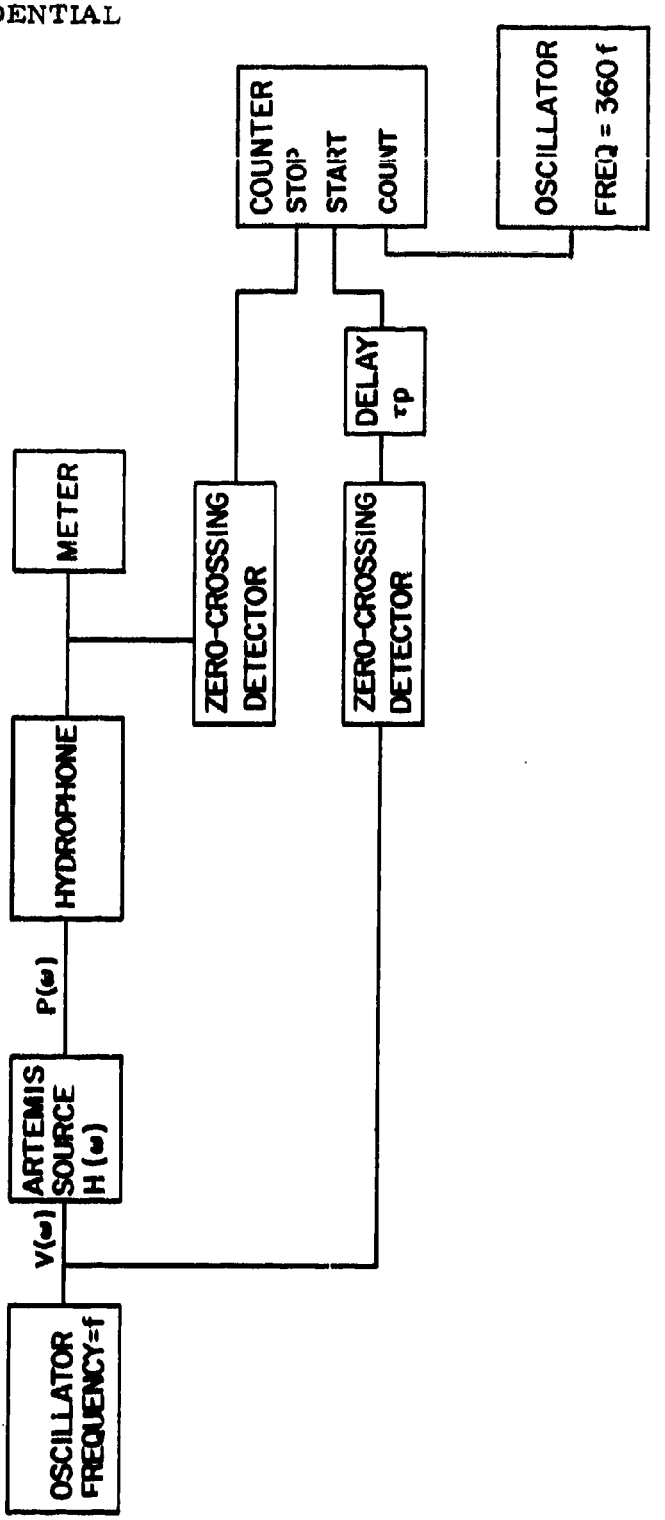

Fig. 13 - Instrumentation for measurement of transfer function using sine waves

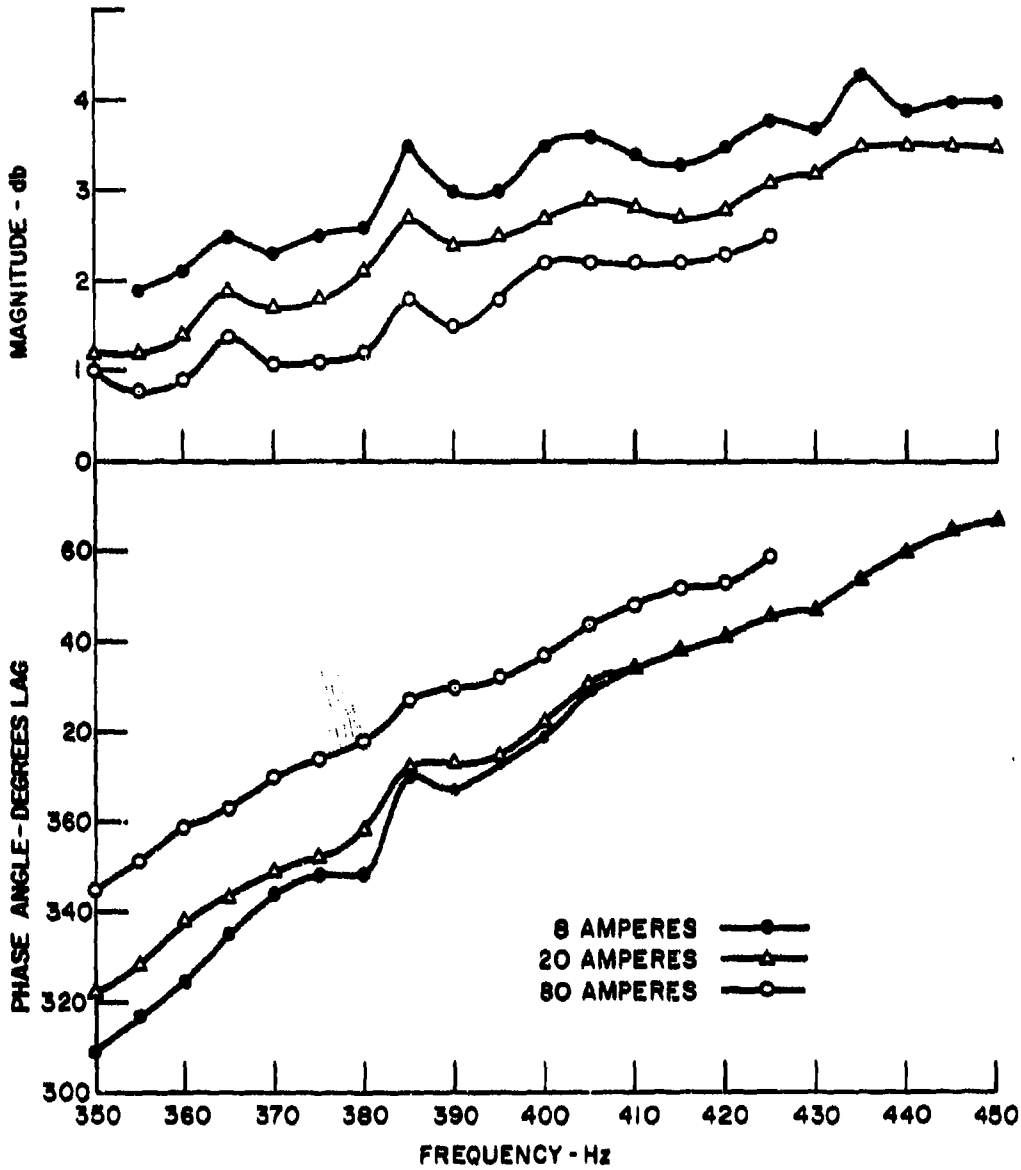

Fig. 14 - Transfer function of the Artemis source for three values of sine wave current

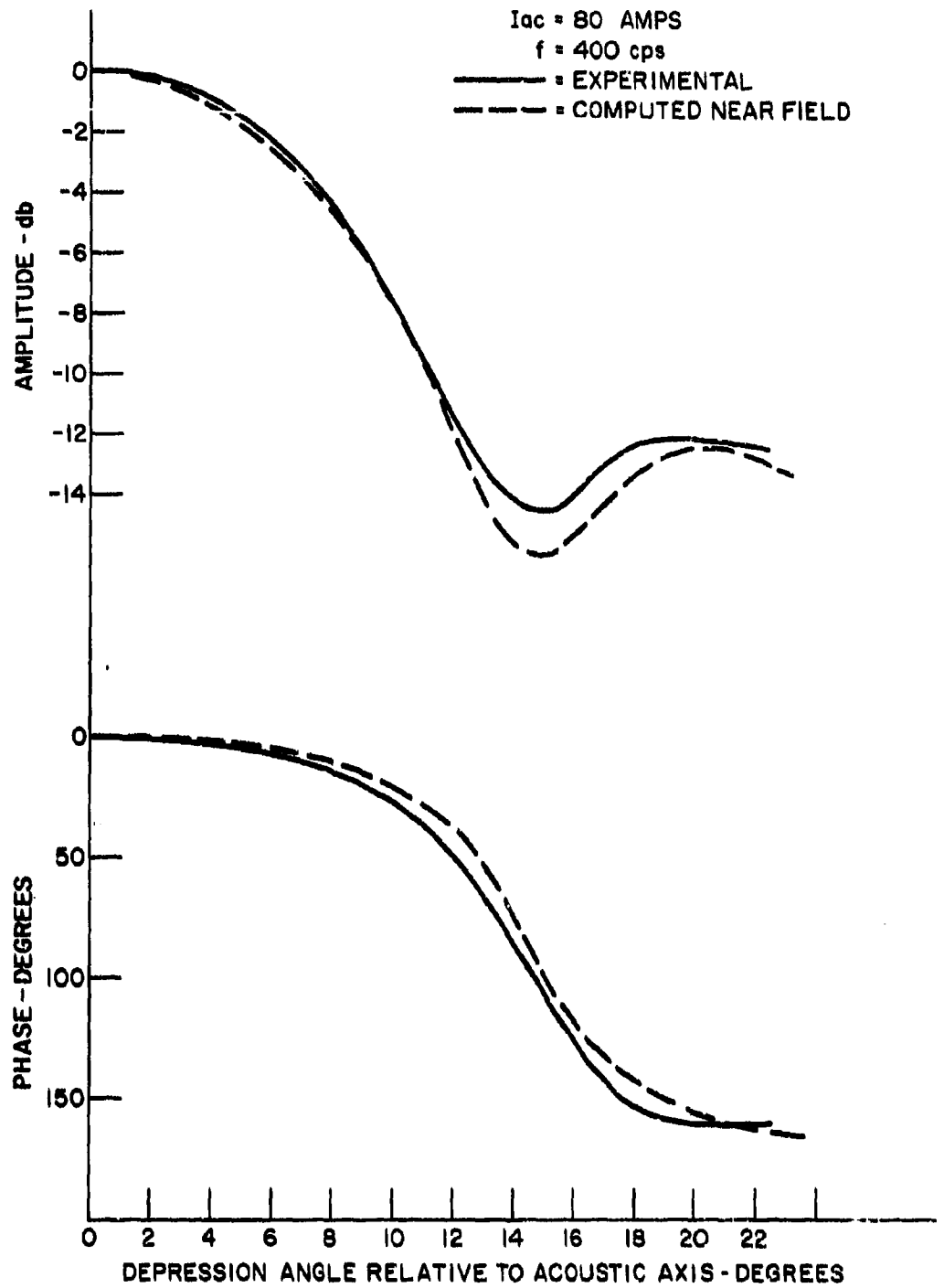

Fig. 15 - Acoustic amplitude and phase characteristics of the Artemis source

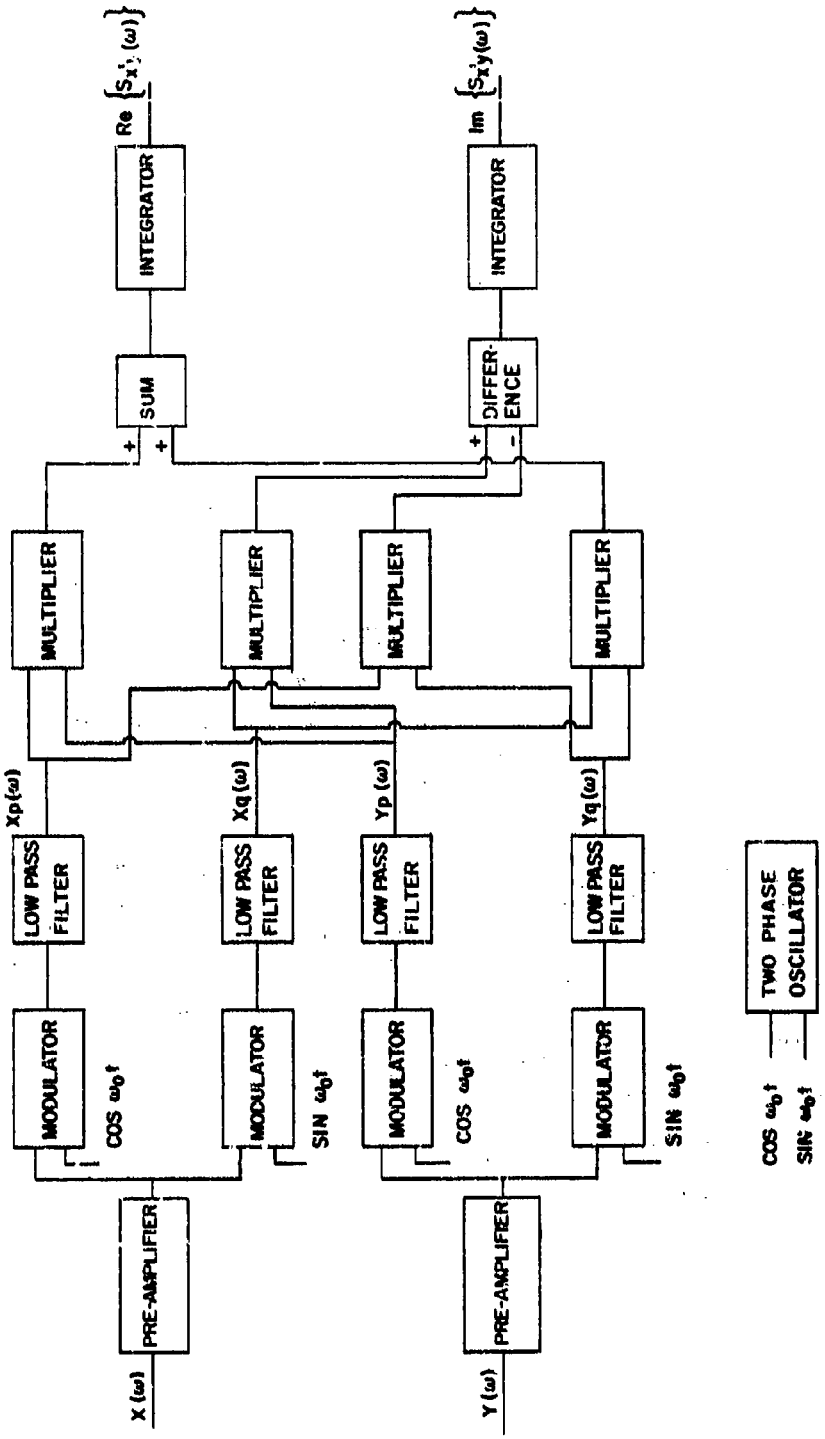

Fig. 16 - Block diagram of cross power spectrum analyser

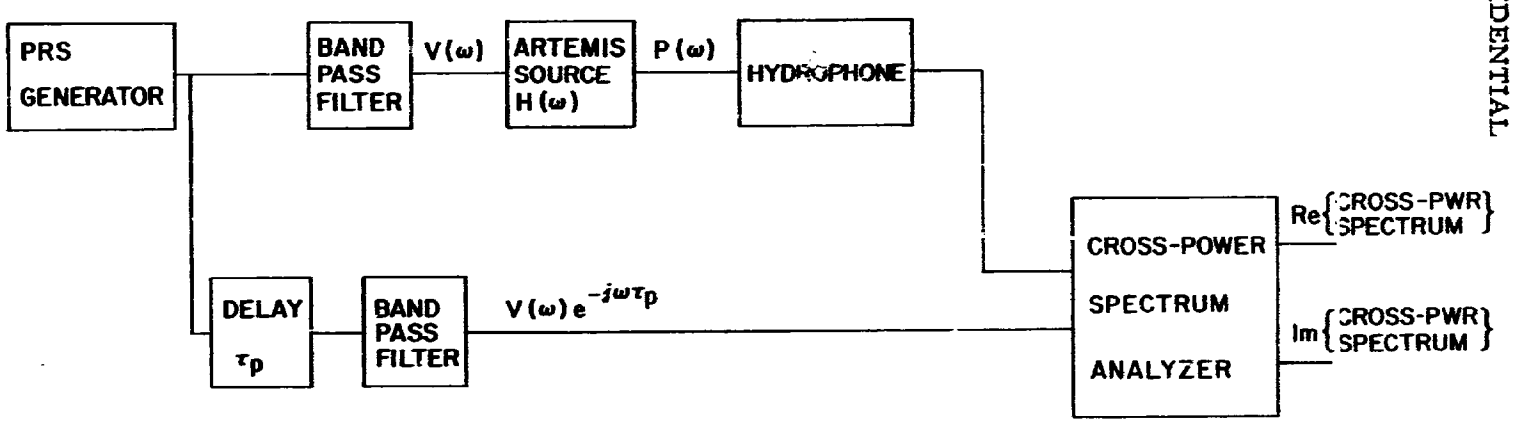

$$S(\omega) = \text{CROSS-POWER SPECTRUM}$$

$$S(\omega) = \left[V(\omega)\, e^{-j\omega\tau p}\right]\left[p(\omega)\right]^* = \left[V(\omega)\, e^{-j\omega\tau p}\right]\left[H(\omega)^*\ V(\omega)^*\right]$$

$$S(\omega) = \left|V(\omega)\right|^2 e^{-j\omega\tau p}\ H(\omega)^*$$

$$S(\omega) = \left|V(\omega)\right|^2 Ho(\omega)^*$$

Fig. 17 - Block diagram of instrumentation used for transfer function measurement with pseudo-random signals

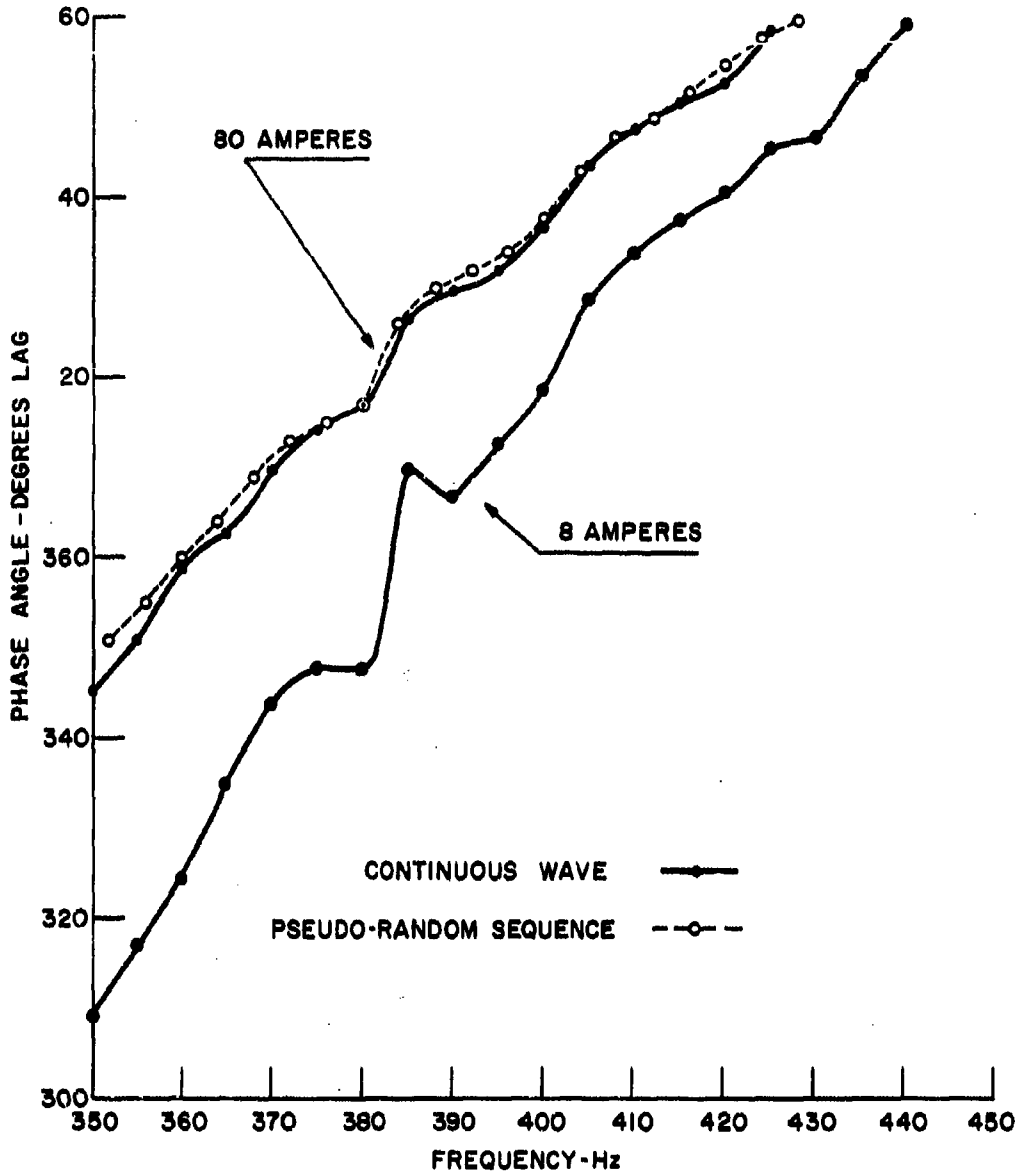

Fig. 18 - Comparison of transfer function phase of the Artemis source as measured with sinusoidal and pseudo-random signals

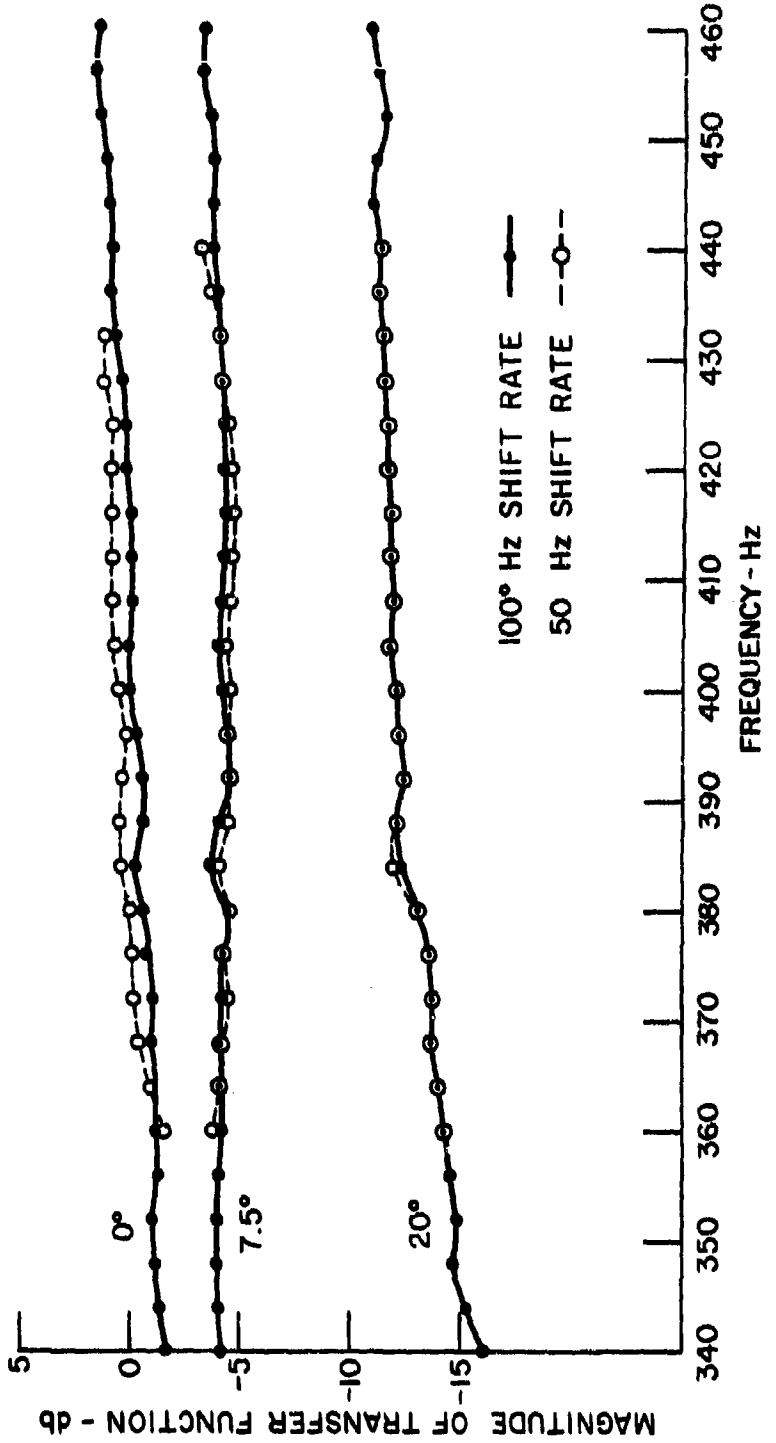

Fig. 19 - Magnitude of the Artemis source transfer function for three angles relative to the acoustic axis

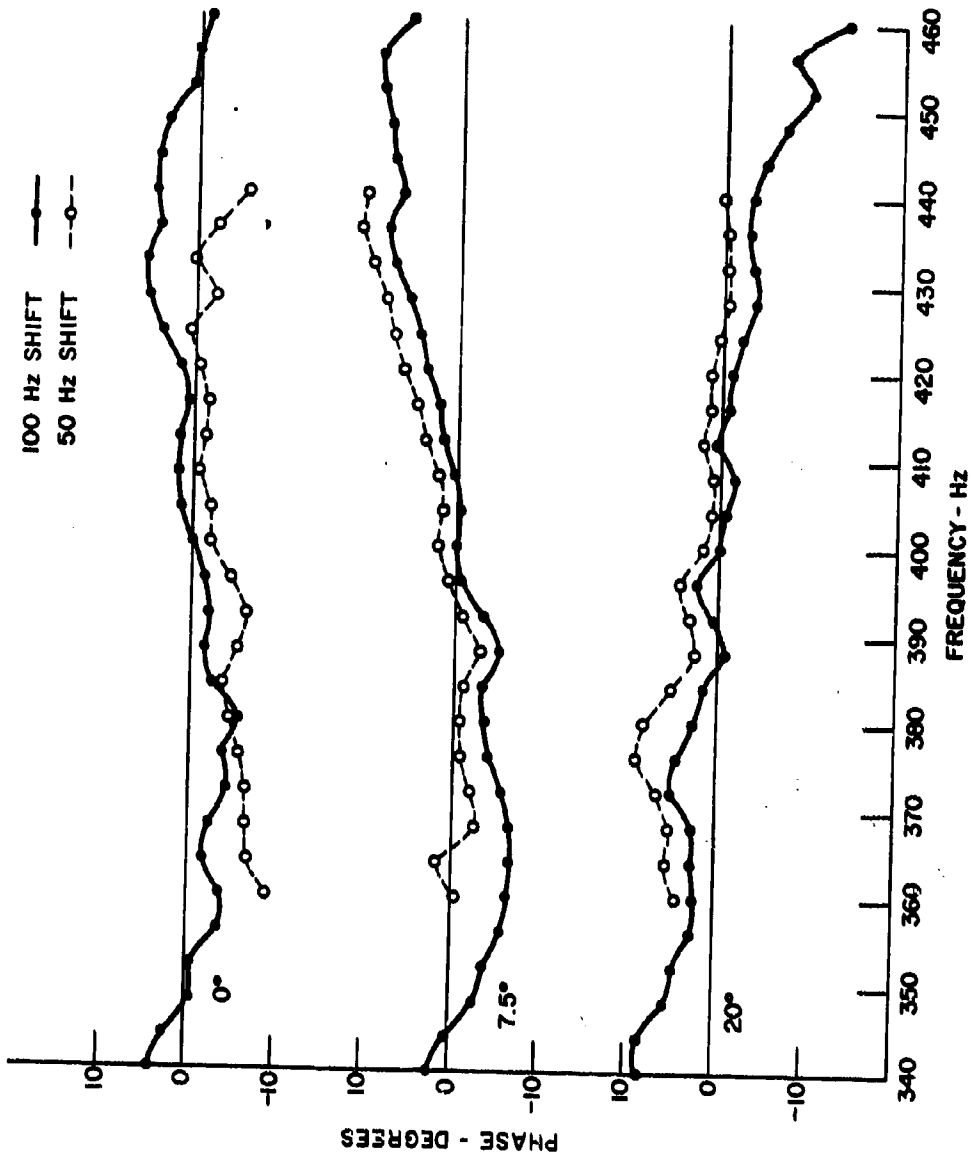

Fig. 20 - Phase of the Artemis source transfer function for three angles relative to the acoustic axis

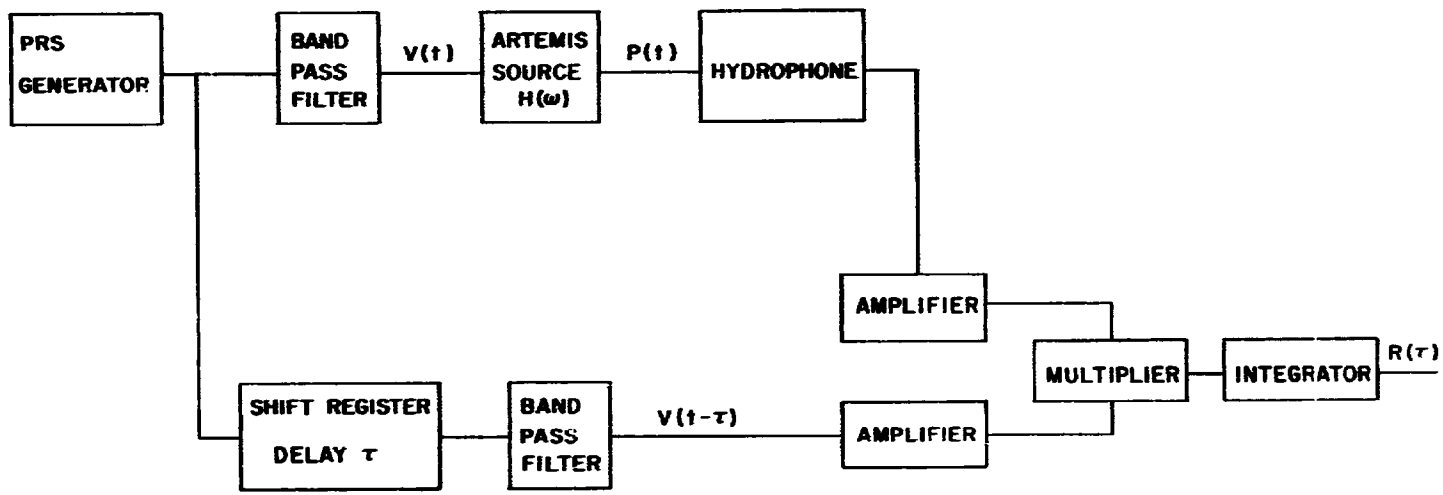

$$R(\tau) = \int_0^T p(t)\ V(t-\tau)\,dt \qquad \text{CROSS-CORRELATION FUNCTION}$$

$$\rho(\tau) = \frac{\int_0^T p(t)\ V(t-\tau)\,dt}{\sqrt{\int_0^T p(t)^2\,dt \int_0^T V(t)^2\,dt}} \qquad \text{NORMALIZED CROSS-CORRELATION FUNCTION}$$

Fig. 21 - Instrumentation used for measurement of the cross correlation function between the input and output of the Artemis source

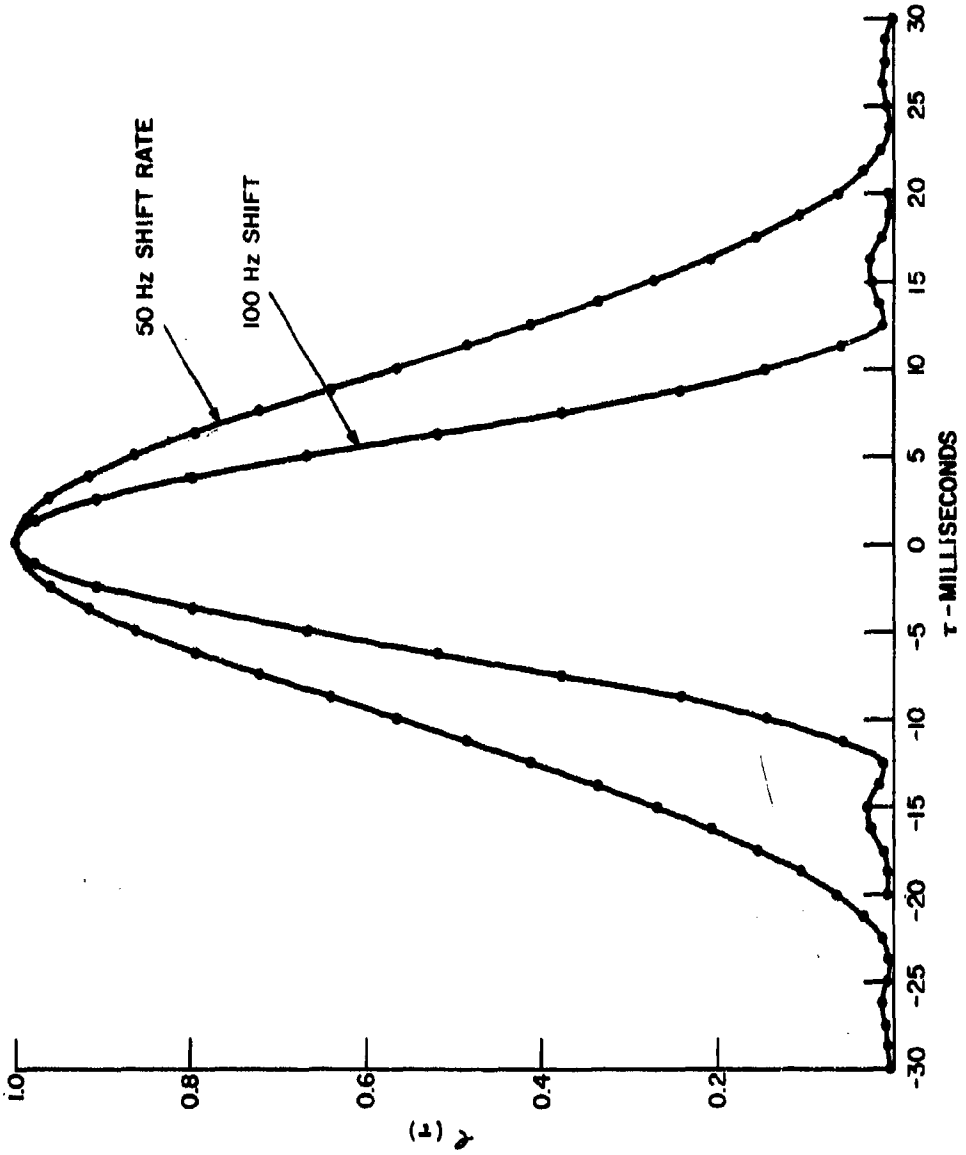

Fig. 22 - Normalized cross correlations between the input and output of the Artemis source for two pseudo-random sequences

UNCLASSIFIED
Security Classification

DOCUMENT CONTROL DATA - R & D

(Security classification of title, body of abstract and indexing annotation must be entered when the overall report is classified)

1. ORIGINATING ACTIVITY *(Corporate author)* Naval Research Laboratory Washington, D. C. 20390	2a. REPORT SECURITY CLASSIFICATION Confidential 2b. GROUP 4

3. REPORT TITLE

POWER LIMITATIONS AND FIDELITY OF ACOUSTIC SOURCES

4. DESCRIPTIVE NOTES *(Type of report and inclusive dates)*

An interim report on one phase of the problem.

5. AUTHOR(S) *(First name, middle initial, last name)*

Ferris, R. H., and Hunsicker, F. L.

6. REPORT DATE	7a. TOTAL NO. OF PAGES	7b. NO. OF REFS
	52	5

8a. CONTRACT OR GRANT NO. NRL Problem S01-23 b. PROJECT NO. RF 101-03-44-4066 c. Bureau Problem SF 101-03-16-11223 d.	9a. ORIGINATOR'S REPORT NUMBER(S) NRL Memorandum Report 1730 9b. OTHER REPORT NO(S) *(Any other numbers that may be assigned this report)*

10. DISTRIBUTION STATEMENT

To be made available to those having proper security clearance and need to know.

11. SUPPLEMENTARY NOTES	12. SPONSORING MILITARY ACTIVITY ONR and Naval Electronic Systems Command, Washington, D. C.

13. ABSTRACT (Unclassified)

The generation of a high-intensity acoustic field which is a faithful replica, or at least a known function, of the input signal is a prime requirement in modern active sonar systems. Most sonar signals in use are modulated sine waves. Therefore, transducers must be capable of efficiently transforming this type of signal. It is evident that design criteria and test procedures based on steady-state sine-wave signals are not adequate. The potential gain in sonar performance to be realized by maximizing signal power without distortion merits increased effort addressed to this problem.

This report is intended to point out some of the problems associated with the generation of maximum-energy acoustic fields by large multielement sources and to suggest techniques of analysis and testing. The use of electrical analog analysis of power-limiting factors in transducer elements appears to be an attractive method if a means can be developed for estimating the range of acoustic-loading values experienced by elements in an active array.

A description of calibration procedures used and results obtained in tests of the ARTEMIS acoustic source are presented to serve as an example of proposed test methods.

DD FORM 1 NOV 65 1473 (PAGE 1)

S/N 0101-807-6801

UNCLASSIFIED
Security Classification

UNCLASSIFIED
Security Classification

14 KEY WORDS	LINK A ROLE	LINK A WT	LINK B ROLE	LINK B WT	LINK C ROLE	LINK C WT
Acoustic sources						
Power limitations						
High-intensity sonar acoustic field						
Sonar						
Sound transducers						
Electrical analog analysis						
Calibration procedures for ARTEMIS						

DD FORM 1 NOV 65 1473 (BACK)
(PAGE 2)

UNCLASSIFIED
Security Classification

UNITED STATES GOVERNMENT

Memorandum

7100-016

DATE: 22 January 2004

REPLY TO ATTN OF: Burton G. Hurdle (Code 7103)

SUBJECT: REVIEW OF REF (A) FOR DECLASSIFICATION

TO: Code 1221.1

REF: (a) "Project ARTEMIS High Power Acoustic Source", A.T. McClinton, R.H. Ferris, W.A. Herrington, Sound Div., NRL Memo Report 1205, 3 Aug 1961 (U)
(b) "Project ARTEMIS High Power Acoustic Source Second Interim Report on Acoustic Performance", A.T. McClinton and R.H. Ferris, Sound Division, NRL Memo Report 1214, 19 September 1961 (U)
(c) "Project ARTEMIS High Power Acoustic Source Third Interim Report on Acoustic Performance", A.T. McClinton, R.H. Ferris, Sound Division, NRL Memo Report 1273, 23 April 1962 (U)
(d) "Project ARETMIS High Power Acoustic Source Effect of Transducer Element Electrical Connection on Interaction in a Consolidated Array", A.T. McClinton, Sound Division, NRL Memo Report 1323, 4 June 1962 (U)
(e) "Test of Project ARTEMIS Source", R.H. Ferris, Sound Division, NRL Memo Report 1648, 15 September 1965 (U)
(f) "Power Limitations and Fidelity of Acoustic Sources", R.H. Ferris and F.L. Hunsicker, Sound Division, NRL Memo Report 1730, November 1966 (U)
(g) "Project ARTEMIS Acoustic Source Acoustic Test Procedure", R.H. Ferris and C.R. Rollins, Sound Division, NRL Memo Report 1769, 5 June 1967 (U)
(h) "Calibration of the ARTEIS Source and Receiving Array on the Mission Capistrano", M. Flato, Acoustics Div., NRL Memo Report 2712, Dec 1973 (U)
(i) "Theoretical Interaction Computations for Transducer Arrays, Including the Effects of Several Different Types of Electrical Terminal Connections", R.V. Baier, Sound Division, NRL Report 6314, 7 October 1965 (U)
(j) "Project ARTEMIS Acoustic Source Summary Report", NRL Report 6535, September 1967 (U)

1. References (a) thru (j) are a series of reports on Project ARTEMIS Reports by the Sound Division that have previously been declassified.

2. The technology and equipment of reference (a) have long been superseded. The current value of these papers is historical

3. Based on the above, it is recommended that reference (a) be available with no restrictions.

BURTON G. HURDLE
NRL Code 7103

CONCUR:

Edward R. Franchi 1/23/2004
E.R. Franchi Date
Superintendent, Acoustics Division

CONCUR:

Tina Smallwood 1/28/04
Tina Smallwood Date
NRL Code 1221.1